npj | parkinson's disease

Article

Published in partnership with the Parkinson's Foundation

https://doi.org/10.1038/s41531-025-01135-4

Capsaicin and nicotine alleviate MPTP induced olfactory dysfunction by suppressing cGAS/TBK1/STING and MAPK mediated neuroinflammation

Jingjing Wei[1,2], Linhai Wang[1,2], Dingzhong Wang[2], Weiwei Chen[3], Lulu Guo[2], Mengqian Ren[1,2], Fangxin Guo[3], Sisi Ruan[1,2], Hangcui Hu[3], Yao Zheng[3], Siqi Nan[1,2], Zhiwen Xu[3], Yan Li[1], Hang Yuan[1], Jian Mao[2] ✉, Yan Xu[3] ✉ & Jianping Xie[2]

Olfactory dysfunction serves as a potential early diagnostic biomarker for Parkinson's disease (PD), providing essential evidence for investigating PD pathogenesis and developing neuroprotective strategies. Capsaicin (CAP) and nicotine (Nic), pungent flavor compounds derived from *Solanaceae* plants, exhibit anti-inflammatory properties. Epidemiological studies indicate that higher levels of chili pepper consumption and smoking are inversely associated with PD risk. However, the mechanisms of CAP and Nic against PD-related olfactory dysfunction remain unclear. In this study, we observed that CAP and Nic ameliorated olfactory dysfunction in MPTP intranasal-treated PD mice and alleviated dopaminergic damage in key brain regions including the olfactory bulb, anterior olfactory nucleus, striatum and substantia nigra. Both compounds suppressed microglial activation in these regions, downregulated IL-6 expression, and upregulated TGF-β protein levels. Furthermore, our findings demonstrated that CAP and Nic could effectively mitigate MPTP-induced olfactory deficits by attenuating neuroinflammation mediated through the cGAS/TBK1/STING and MAPK signaling.

Parkinson's disease (PD) is one of the most common neurodegenerative disorders characterized by motor symptoms such as bradykinesia, rigidity, tremor, postural instability, etc., but it is also well known that a lot of non-motor symptoms, such as olfactory dysfunction, constipation, and sleep behavior disorder, often precede motor symptoms[1]. The current diagnostic criteria for PD are mostly based on motor symptoms. Among non-motor symptoms, olfactory dysfunction is commonly considered in the prodromal stage of PD, affecting 75-90% of the patients[2]. Therefore, the detection of olfactory impairment may contribute to the accurate diagnosis of the prodromal phase of PD and the prediction of the risk of disease progression[3].The pathological hallmarks of sporadic PD are the loss of dopaminergic neurons in the substantia nigra pars compacta (SNc) in association with Lewy bodies (LBs) and Lewy neurites, both of which are mainly composed of aggregated α-synuclein (α-syn)[4–6]. The Braak hypothesis and the "dual-hit hypothesis" propose that α-syn begins its spread from the olfactory bulb and propagates to the temporal cortex[7,8]. Moreover, Nolwen et al. demonstrated that α-syn pathology propagates through the olfactory system, which may be the cause of olfactory dysfunction[7,9]. Over the past few decades, the neurotoxin 1-methyl-4-phenyl-1,2,3,6-tetrahydropyridine (MPTP) has emerged as a widely utilized method for modeling PD[10]. The nasal mucosa boasts structural features such as a large surface area and a porous endothelial membrane. The distribution region of olfactory receptors is adjacent to the central nervous system, and the blood-brain barrier (BBB) in the olfactory bulb region is relatively weak, facilitating the passage of MPTP. These characteristics render intranasal administration an ideal approach for constructing animal models of PD[11–13].

Capsaicin (CAP, trans-8-methyl-N-vanillyl-6-nonenamide), a bioactive alkaloid derived from chili peppers (Capsicum spp., *Solanaceae*), is the primary compound responsible for their pungency[14]. Historically cultivated since the 5th millennium BC, chili peppers have been integral to global cuisines, with CAP ubiquitously consumed via traditional dishes and processed foods[15,16]. Beyond its culinary role, CAP exhibits multifaceted therapeutic properties. As a phytomedical compound, CAP has been demonstrated to have analgesic, antioxidant, anti-inflammatory,

[1]Flavour Science Research Center, College of Chemistry, Zhengzhou University, Zhengzhou, China. [2]Beijing Life Science Academy (BLSA), Beijing, China. [3]School of Basic Medical Sciences, College of Medicine, Zhengzhou University, Zhengzhou, China.
✉e-mail: 20012188mj@163.com; yxu@zzu.edu.cn

anti-cancer, cardio-protective, metabolic modulation effects, etc[16]. Nicotine (Nic, (*S*)-3-(1-methylpyrrolidin-2-yl) pyridine), the principal alkaloid of Nicotiana tabacum L. (*Solanaceae*), is the primary addictive component of cigarettes and has been intrinsically linked to human societies since its global dissemination in 1492[17,18]. Beyond its stimulant properties, Nic exerts neuroprotection-attenuating neuronal excitotoxicity, potentiating neurotrophic signaling, suppressing neuroinflammation, mitigating oxidative damage, inhibiting apoptosis, etc[19,20]. CAP and Nic are both pungent flavor compounds extracted from plants of the *Solanaceae* family, known for their neuroprotective effects such as anti-inflammatory and anti-apoptotic properties. CAP can reduce oxidative stress and the production of pro-inflammatory mediators, suppresses abnormal activation of astrocytes, and effectively inhibits the release of inflammatory mediators such as ROS, TNF-α, and IL-1β, thus exerting its neuroprotective effects[21]. Furthermore, studies have demonstrated that CAP can also modulate the M1/M2 polarization of microglia, reduce the protein expression levels of pro-inflammatory factors (such as iNOS and IL-1), and decrease cell apoptosis, thereby mitigating the death of dopaminergic neurons in the substantia nigra of PD mice[22]. Epidemiological studies have found that the incidence of PD is lower among smokers[23]. Nic inhibits neuronal damage by suppressing M1 polarization of microglia, reducing the secretion of the pro-inflammatory factor TNF-α, and activating the PI3K-AKT signaling pathway[24]. In PD, Nic can activate α3*/α6* nicotinic acetylcholine receptors (nAChRs), thereby reducing degeneration of dopaminergic neurons in the striatum and substantia nigra and alleviating PD symptoms[25,26]. CAP and Nic exert significant neuroprotective effects in PD through various mechanisms, such as modulating inflammatory responses reducing oxidative stress, and inhibiting neuronal damage, offering potential new strategies for PD treatment.

Mitogen-activated protein kinases (MAPKs) are serine-threonine protein kinases that regulate various cellular activities including proliferation, differentiation, apoptosis, survival, inflammation, and innate immunity[27]. In mammals, MAPKs include c-Jun NH_2-terminal kinase (JNK), p38 MAPK, and extracellular signal-regulated kinase (ERK), compromised MAPK signaling pathways have also been found to play key roles in the pathogenesis of PD[28]. The p38 MAPK pathway is robustly activated in PD models mice and critically drives neuronal cell death through α-synuclein phosphorylation and neuroinflammation[29]. Understanding this signaling axis provides a rational foundation for developing novel MAPK-targeted therapeutics against PD and related neurodegenerative disorders. For instance, L-theanine improves motor deficits in MPTP-induced PD mice by targeting the Wnt/β-catenin signaling pathway-related proteins through the MAPK pathway (p-JNK, p-ERK, and p-p38) and regulating oxidative stress-related factors such as SOD-1, GST, and NO[30]. Nic activates nAChRs to facilitate NGF-Trk receptor binding, inducing tyrosine residue autophosphorylation, this triggers downstream signaling pathways—particularly the MAPK/ERK cascade—to promote neuronal survival, growth, and differentiation synthase[31]. Meanwhile, the cyclic GMP- AMP synthase (cGAS) is a primary cytosolic double- stranded DNA sensor that initiates inflammation in response to infection or sterile tissue damage[32]. Upon DNA binding, cGAS is activated to catalyze the synthesis of 2′,3′-cGAMP, while the stimulator of interferon genes (STING) acts as an adaptor protein coordinated by cGAS to protect the host, the transcription factor IRF3 is phosphorylated by TBK1, which is recruited by activated STING[33]. The cGAS-STING signaling pathway serves as an innate immune sensor and plays an increasingly important role in neuroinflammation, neurodegenerative diseases, cellular senescence, autoimmunity, and autophagy, among other pathological and physiological processes[34,35]. Inhibiting the cGAS-STING pathway has demonstrated potential in preclinical and clinical studies, reducing neuroinflammation and protecting neurons, making it a promising therapeutic target for PD[36]. cGAS-STING pathway was activated during neuro inflammation in MPTP mouse models of PD. cGAS deficiency in microglia, controlled neuroinflammation and neurotoxicity induced by MPTP[37]. 3-n-Butylphthalide alleviates rotenone-induced PD by inhibiting the cGAS-STING pathway and microglial inflammation[38]. However, the neuroprotective mechanisms of CAP and Nic against olfactory dysfunction in PD murine models remain incompletely characterized. Crucially, it is unknown whether they mediate therapeutic effects via the cGAS/TBK1/STING and MAPK signaling pathways, or how microglia-driven neuroinflammation specifically contributes to this process.

In this study, we established a PD mice model with olfactory dysfunction through intranasal administration of MPTP, followed by intervention with CAP and Nic via intraperitoneal injection. The neuroprotective effects of CAP and Nic on PD mice with olfactory dysfunction were evaluated through olfactory and motor behavioral tests, pathological changes, and neuroinflammatory responses. Furthermore, transcriptomics and proteomics were employed to explore the potential molecular mechanisms underlying the neuroprotective effects of CAP and Nic on PD mice with olfactory dysfunction at both the gene and protein levels.This study provides a new avenue for investigating the neuroprotective properties of pungent flavor compounds (CAP and Nic) in PD.

Results

Capsaicin and nicotine intervention alleviate MPTP-induced olfactory dysfunction

The present data indicates that intranasal administration of MPTP can induce parkinsonism and olfactory dysfunction in mice[11,39,40]. CAP (1 mg/kg) and Nic (2.5 mg/kg) intervention was administered for a 7-day duration in the MPTP-induced PD olfactory dysfunction mouse model to elucidate the neuroprotective mechanism of CAP and Nic (Fig. 1).

On the first day after intranasal administration, olfactory avoidance behavior was tested in MPTP-induced mice. The results (Fig. 2a) showed no significant differences in sniffing time among the saline group, MPTP group, CAP + MPTP group, and Nic+MPTP group in the water and hexanone areas, indicating that no olfactory dysfunction was observed in the mice in different groups on the first day after the intranasal administration. Subsequently, the buried food pellet test was conducted to evaluate olfactory perception ability of mice, the results (Fig. 2b) showed that compared to the saline group, the MPTP group took significantly longer time to find the food, meanwhile, the CAP + MPTP and Nic+MPTP groups respectively took significantly reduced time to find the sweetened cereal compared to the MPTP group (Fig. 2b). Olfactory preference test was used to assess the odor perception and discrimination abilities of mice. The results (Fig. 2c, d) showed that compared to the saline group, the MPTP group spent significantly less time sniffing mouse urine (preferred odor), the difference in sniffing time between water (neutral odor) and mouse urine was significantly reduced. Whereas, the CAP + MPTP and Nic+MPTP groups took significantly increased sniffing time for mouse urine compared to the MPTP group. Furthermore, the block test was conducted to evaluate the ability to discriminate social odors of mice, the results (Fig. 2e, f) showed that compared to the saline group, the MPTP group spent significantly less time sniffing the new odor, and the ratio of new odor to self-odor was significantly reduced. Meanwhile, the CAP + MPTP and Nic+MPTP groups showed significantly increased sniffing time for the new odor, and the new odor/self-odor ratio was significantly higher in the groups compared to the MPTP group. The olfactory avoidance test was repeated on day 17, the results (Fig. 2g, h) showed that compared to the saline group, the MPTP group spent significantly less time sniffing in the water area and striking more time in the hexanone area, with a significantly reduced difference in sniffing time between the two areas. Meanwhile, the CAP + MPTP and Nic+MPTP groups showed significant alleviation of these effects compared to the MPTP group.

All the above olfactory behavioral tests indicated that MPTP-induced PD mice developed olfactory dysfunction, and intervention with CAP and Nic significantly improved olfactory impairment in PD mice. Finally, the go/no-go olfactory training system was used to evaluate the comprehensive abilities of mice in odor detection, discrimination, learning, and memory. The results (Fig. 2i–k) showed that on the first day of the go/no-go trial, compared to the saline group, the MPTP group exhibited a significantly lower correct rate (licking water in response to isoamyl acetate and correctly

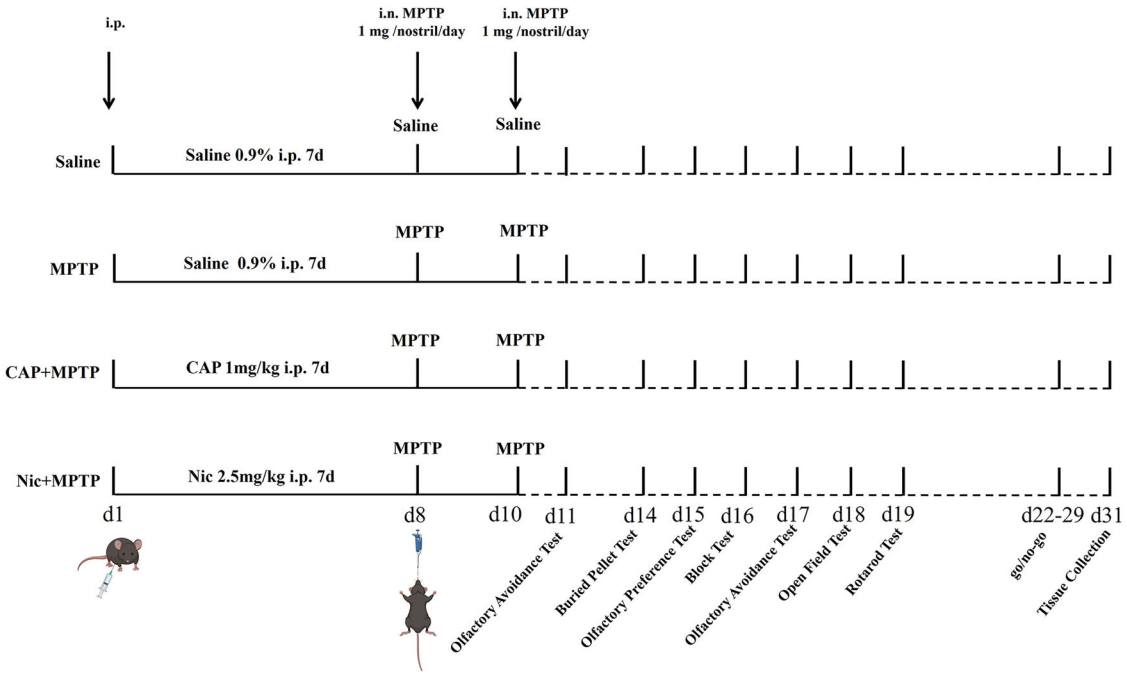

Fig. 1 | Schematic diagram of the MPTP-induced mice model.

avoiding heptanone). Across five sessions, the correct rate of MPTP group was consistently lower than that of the saline group, and the correct avoidance rate of MPTP group was significantly lower than that of the saline group. These results indicated that MPTP-induced PD mice developed olfactory dysfunction, and Nic intervention significantly improved the abilities in odor detection of mice, discrimination, learning, and memory. Although the CAP intervention group showed a trend of increased correct rate, the improvement was not significant. On the second and third days of the go/no-go test, the CAP and Nic intervention groups still showed this trend compared to the MPTP group, but the improvement was not significant (Fig. 2l, m).

Capsaicin and nicotine intervention alleviate MPTP-induced anxiety-like behavior and locomotor deficit

The open field test was conducted to evaluate anxiety and motor abilities in mice. The results (Fig. 3a, b) showed that compared to the saline group, the MPTP group exhibited a significant reduction in the proportion of distance traveled in the center zone. Whereas, the CAP + MPTP and Nic+MPTP groups showed a significant increase in the time spent exploring the center zone compared to the MPTP group (Fig. 3a, b). Additionally, compared to the saline group, the MPTP group showed a significant decrease in the total distance traveled in the open field, while the CAP + MPTP and Nic+MPTP groups exhibited a significant increase in the total distance traveled compared to the MPTP group. Furthermore, the rotarod test was used to assess motor coordination in mice, with the average fall time as the evaluation criterion. The results (Fig. 3d) showed that compared to the saline group, the MPTP group had a significantly reduced average fall time, while the CAP + MPTP and Nic+MPTP groups separately showed a significant increase in average fall time compared to the MPTP group. These results indicate that the MPTP-induced PD mouse model with olfactory dysfunction exhibited anxiety-like behavior and motor impairments. Whereas, intervention with CAP and Nic significantly alleviated anxiety-like behavior and motor deficits in PD mice with olfactory dysfunction.

Capsaicin and nicotine intervention alleviate MPTP-induced degeneration of dopaminergic neurons

A defining feature of PD is the degeneration of dopaminergic neurons in the SNc, leading to motor impairments. Studies suggest that the olfactory tubercle and other mesolimbic regions receive dopaminergic input from the ventral tegmental area, and dopamine deficiency in these regions may be a critical factor contributing to olfactory loss in PD patients[41]. To investigate the effects of CAP and Nic on dopaminergic neurons in PD mice with olfactory dysfunction, immunohistochemical staining for tyrosine hydroxylase (TH) was performed in the olfactory bulb, olfactory tubercle, striatum and substantia nigra regions. The results (Fig. 4a-e) showed that compared to the saline group, the MPTP group exhibited a significant reduction in TH expression levels in the olfactory bulb, olfactory tubercle, striatum and substantia nigra regions separately. Meanwhile, the CAP + MPTP and Nic+MPTP groups showed significantly increased TH expression levels compared to the MPTP group in the four brain regions separately. These results suggest that CAP and Nic intervention can effectively alleviate the degeneration of dopaminergic neurons in the olfactory bulb, olfactory tubercle, striatum and substantia nigra regions of PD mice.

Capsaicin and nicotine intervention inhibit MPTP-induced activation of microglia

The involvement of microglia in neuroinflammation plays a pivotal role in the progression of PD[42,43]. CAP and Nic may exert neuroprotective effects through the anti-inflammatory properties[44,45]. We evaluated the effects on neuroinflammation of CAP and Nic in MPTP-induced mouse model of PD with olfactory dysfunction. Immunofluorescence revealed microglial activated—defined by $CD68^+/Iba1^+$ co-localization, Iba1 positive cells and morphological alterations—across multiple brain regions: the olfactory bulb (glomerular, external plexiform and granular cell layers), anterior olfactory nucleus, striatum and substantia nigra. The results (Figs. 5a, b, d, h, 6a, b, d and 7a, b, d, h) showed that compared to the saline group, the MPTP group exhibited a significant increase in the expression of $CD68^+/Iba1^+$ co-expression. Morphological analysis (Figs. 5a−j, 6a−j and 7a−j) revealed that microglia in the MPTP group displayed a significant increase in activated microglia, reduced branching nodes, and shortened cell processes. Notably, the CAP + MPTP and Nic+MPTP groups cotreatment counteracted MPTP-induced effects, attenuate $CD68^+/Iba1^+$ co-expression and reversing microglial activation—as evidenced by reduced activated microglia, increased branching points, and elongated processes relative to the MPTP group. These findings indicate that CAP and Nic intervention may

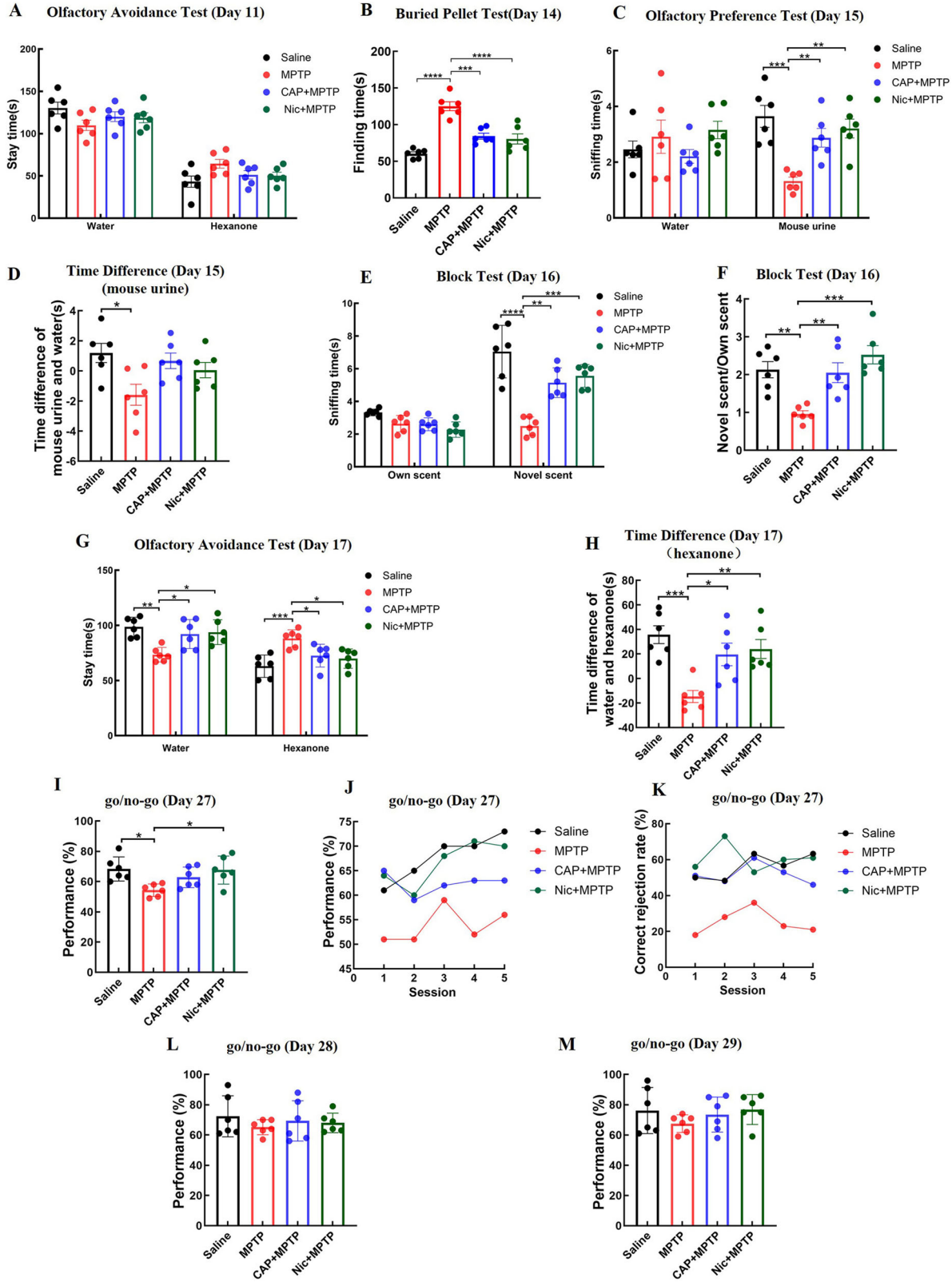

Fig. 2 | Effects of CAP and Nic intervention on olfactory behavior in MPTP-induced mice. a Olfactory avoidance test; **b** Buried food pellet test; **c** Olfactory preference test; **d** Sniffing time difference in the olfactory preference test; **e** Block test; **f** Sniffing time ratio in the block test; **g** Olfactory avoidance test on day 17; **h** Sniffing time difference in the olfactory avoidance test; **i** go/no-go test day 1; **j** Accuracy rate across 5 sessions of the go/no-go test; **k** Rejection rate across 5 sessions of the go/no-go test; **l** go/no-go test day 2; **m** go/no-go test day 3. The data are expressed as the mean ± S.E.M. ($n = 6$ mice per group for a-m. Statistical analyses were performed by one-way ANOVA followed by Tukey's multiple comparison test. $^{*}p < 0.05$, $^{**}p < 0.01$, $^{***}p < 0.001$, $^{****}p < 0.0001$.

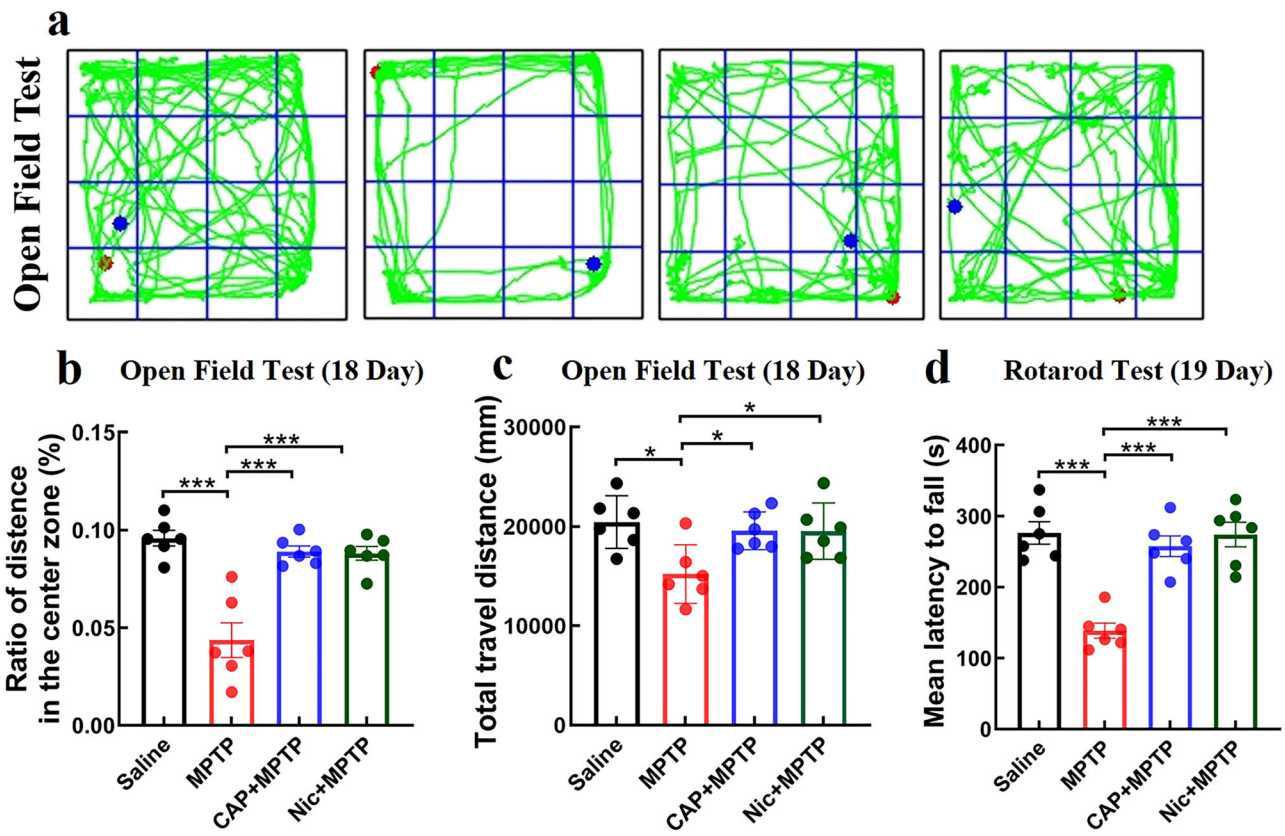

Fig. 3 | Effects of CAP and Nic intervention on anxiety-like behavior and locomotor deficit in MPTP-induced mice. a Representative diagram of the open field test; **b** The distance traveled in the center zone relative to the total distance in the open field test; **c** The total distance traveled in the open field test; **d** The average time taken to fall in the rotarod test. ($n = 6$ mice per group for **a**–**d**). Statistical analyses were performed by one-way ANOVA followed by Tukey's multiple comparison test. $^{*}p < 0.05$, $^{***}p < 0.001$.

suppress microglia-mediated neuroinflammation in the olfactory bulb, anterior olfactory nucleus, striatum and substantia nigra regions of PD mice.

Capsaicin and nicotine intervention inhibit MPTP-induced pro-inflammatory and promote anti-inflammatory factor expression

The release of inflammatory factors mediated by microglial polarization plays a crucial regulatory role in the pathological progression of PD[46,47]. We measured the protein expression levels of the pro-inflammatory factor IL-6 and the anti-inflammatory factor TGF-β in the olfactory bulb, striatum and substantia nigra regions. The results (Fig. 8a-i) showed that compared to the saline group, the MPTP group exhibited a significant increase in IL-6 protein expression and a significant decrease in TGF-β protein expression. Whereas, the CAP + MPTP and Nic+MPTP groups showed significantly reduced IL-6 levels and significantly increased TGF-β levels compared to the MPTP group.These findings suggest that CAP and Nic intervention may suppress the protein expression levels of the pro-inflammatory cytokine IL-6 while promoting the expression of the anti-inflammatory cytokine TGF-β in the olfactory bulb, striatum and substantia nigra regions of PD mice. (Uncropped and unprocessed blot scans in the Supplementary Information).

Molecular characteristics and functional analysis of proteomics

To explore the molecular mechanisms responsible for the neuro protective effects of CAP and Nic in the PD mice model, we used a proteomics approach to investigate the genes and regulatory pathways involved in the neuroprotective effects of CAP and Nic. The results (Fig. 9a–c) showed that in the olfactory bulb samples, in the saline and MPTP groups, 5849 proteins were commonly expressed, in the MPTP and CAP + MPTP groups, 5796 proteins were commonly expressed, in the MPTP and Nic+MPTP groups, 5799 proteins were commonly expressed. In volcano plot analysis in the olfactory bulb (Fig. 9d–e), we discovered 131 proteins exhibited altered expression levels between the saline and MPTP groups, with 63 proteins upregulated and 68 proteins downregulated. Between the MPTP and CAP + MPTP groups, 139 proteins showed changes in expression levels, with 57 proteins upregulated and 82 proteins downregulated. Between the MPTP and Nic+MPTP groups, 401 proteins exhibited altered expression levels, with 97 proteins upregulated and 304 proteins downregulated. Gene Ontology (GO) functional enrichment analysis of these significantly differential expression proteins (Fig. 9g–i) revealed that the MAPK signaling pathway was significantly enriched, suggesting that this pathway may play a key role in the neuroprotective mechanisms of CAP and Nic intervention in PD. Additional quality control metrics of mass spectrometry and Kyoto Encyclopedia of Genes and Genomes (KEGG) signaling pathways in the olfactory bulb region are shown in the figure (Supplementary Information Fig. 2).

Molecular characteristics and functional analysis of transcriptomic

Furthermore, transcriptomic analysis was also conducted on the olfactory bulb region to investigate the genes and regulatory pathways associated with the neuroprotective effects of CAP and Nic in the PD mice model. In volcano plot analysis of the olfactory bulb (Fig. 10a–c) showed that, compared to the saline group, the MPTP group exhibited 43 significantly upregulated genes and 16 significantly downregulated genes. In contrast, the CAP + MPTP group displayed 5 significantly upregulated genes and 4 significantly downregulated genes, while the Nic+MPTP group showed 21 significantly upregulated genes and 5 significantly downregulated genes compared to the MPTP group. KEGG functional enrichment analysis of the differentially expressed genes (Fig. 10d–f) revealed significant enrichment of the MAPK signaling pathway, suggesting that this pathway may play a key

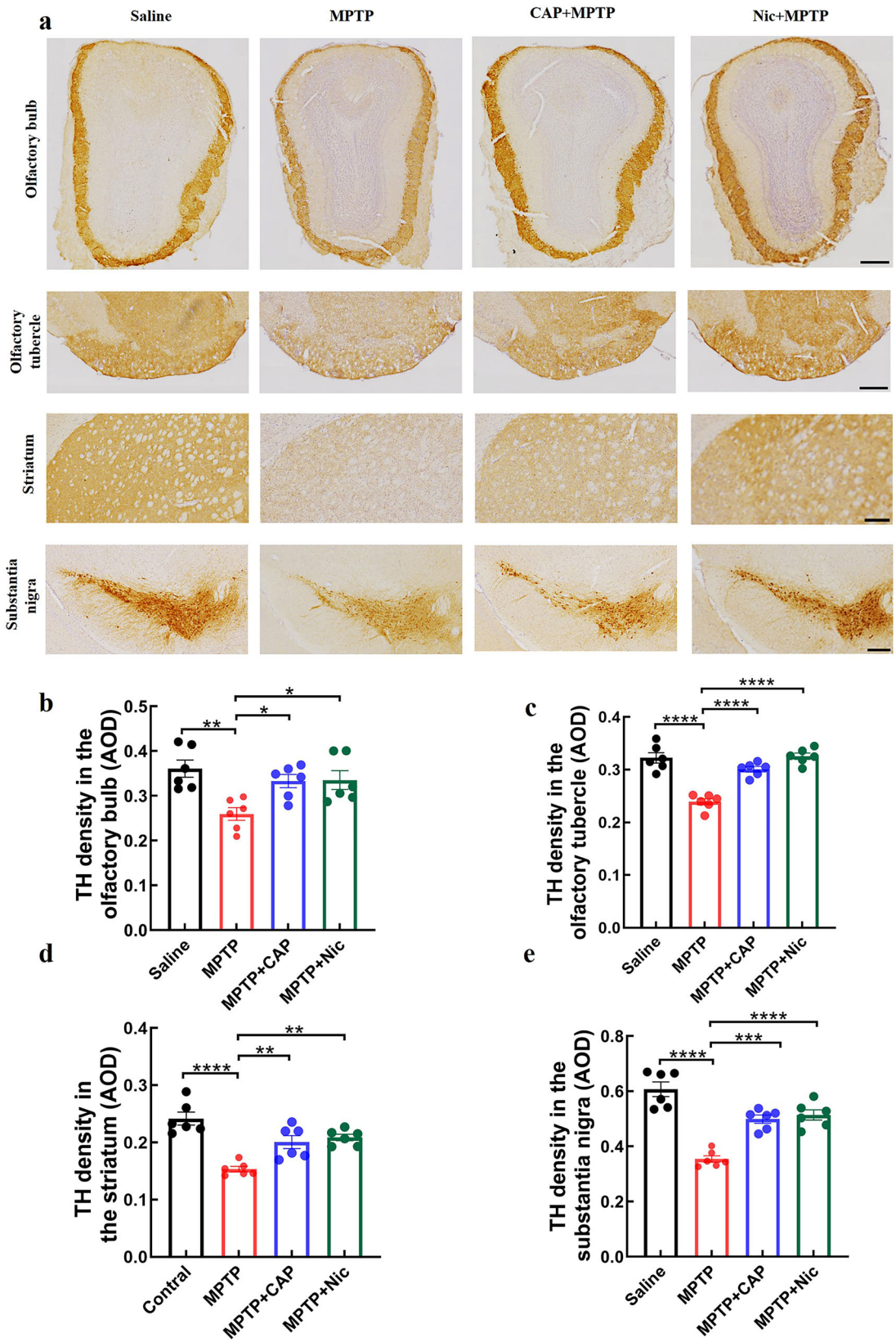

Fig. 4 | Effects of CAP and Nic intervention on dopaminergic neurons in MPTP-induced mice. a Representative pictures displaying staining of TH in the olfactory bulb, olfactory tubercle regions, striatum and substantia nigra; **b** The average optical density of TH in the olfactory bulb region; **c** The average optical density of TH in the olfactory tubercle region. **d** The average optical density of TH in the striatum region; **e** The average optical density of TH in the substantia nigra region. Scale bar for the olfactory bulb = 200 μm; olfactory tubercle = 150 μm. striatum = 25 μm; substantia nigra = 100 μm. ($n = 6$ mice per group for **a**–**e**). Statistical analyses were performed by one-way ANOVA followed by Tukey's multiple comparison test. $^{*}p < 0.05$, $^{**}p < 0.01$, $^{***}p < 0.001$, $^{****}p < 0.0001$.

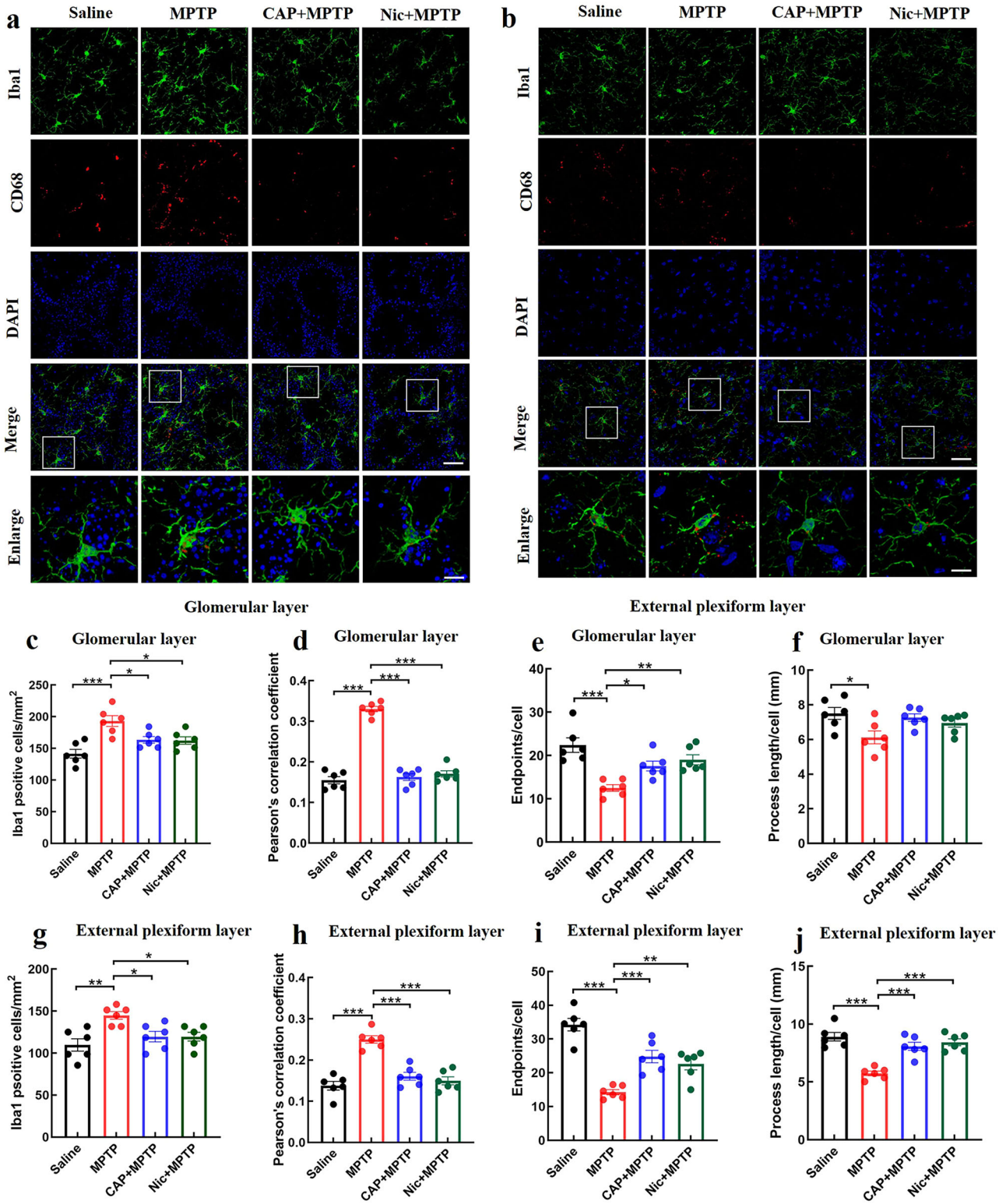

Fig. 5 | Effects of CAP and Nic on microglia in the olfactory bulb of MPTP-induced mice. a Representative immunofluorescence images of Iba1 and CD68 in the glomerular layer of the olfactory bulb; **b** Representative immunofluorescence images of Iba1 and CD68 in the external plexiform layer of the olfactory bulb; **c** Ibar positive cells in the glomerular layer; **d** Iba1 and CD68 co-localization in the glomerular layer; **e** Iba1 endpoints in the glomerular layer; **f** Iba1 process length in the glomerular layer; **g** Ibar positive cells in the external plexiform layer; **h** Iba1 and CD68 co-localization in the external plexiform layer; **i** Iba1 endpoints in the external plexiform layer; **j** Iba1 process length in the external plexiform layer. Iba1: green; CD68: red; DAPI: blue; Images were captured using a 63× objective, scale bar = 25 μm; enlarge scale bar = 2.5 μm. ($n = 6$ mice per group for **a**–**j**). Statistical analyses were performed by one-way ANOVA followed by Tukey's multiple comparison test. $^{*}p < 0.05$, $^{**}p < 0.01$, $^{***}p < 0.001$.

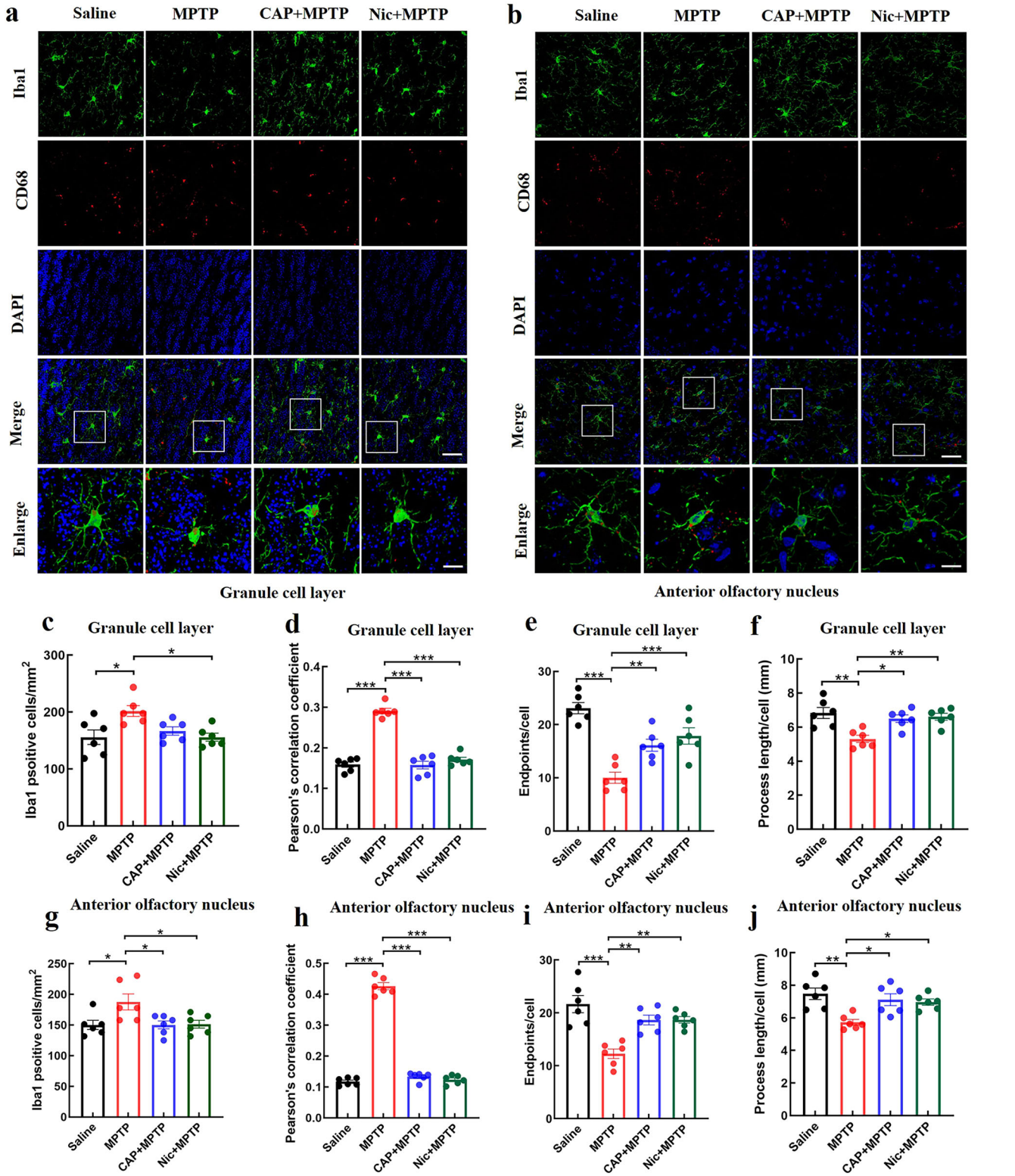

Fig. 6 | Effects of CAP and Nic on microglia in the olfactory bulb and anterior olfactory nucleus of MPTP-induced mice. a Representative immunofluorescence images of Iba1 and CD68 in the granule cell layer of the olfactory bulb; **b** Representative immunofluorescence images of Iba1 and CD68 in the anterior olfactory nucleus; **c** Ibar positive cells in the granule cell layer; **d** Iba1 and CD68 co-localization in the granule cell layer; **e** Iba1 endpoints in the granule cell layer; **f** Iba1 process length in the granule cell layer; **g** Ibar positive cells anterior olfactory nucleus; **h** Iba1 and CD68 co-localization in the anterior olfactory nucleus; **i** Iba1 endpoints in the anterior olfactory nucleus; **j** Iba1 process length in the anterior olfactory nucleus. Iba1: green; CD68: red; DAPI: blue; Images were captured using a 63× objective, scale bar = 25 μm;enlarge scale bar = 2.5 μm. ($n = 6$ mice per group for **a**–**j**). Statistical analyses were performed by one-way ANOVA followed by Tukey's multiple comparison test. $^{*}p < 0.05$, $^{**}p < 0.01$, $^{***}p < 0.001$.

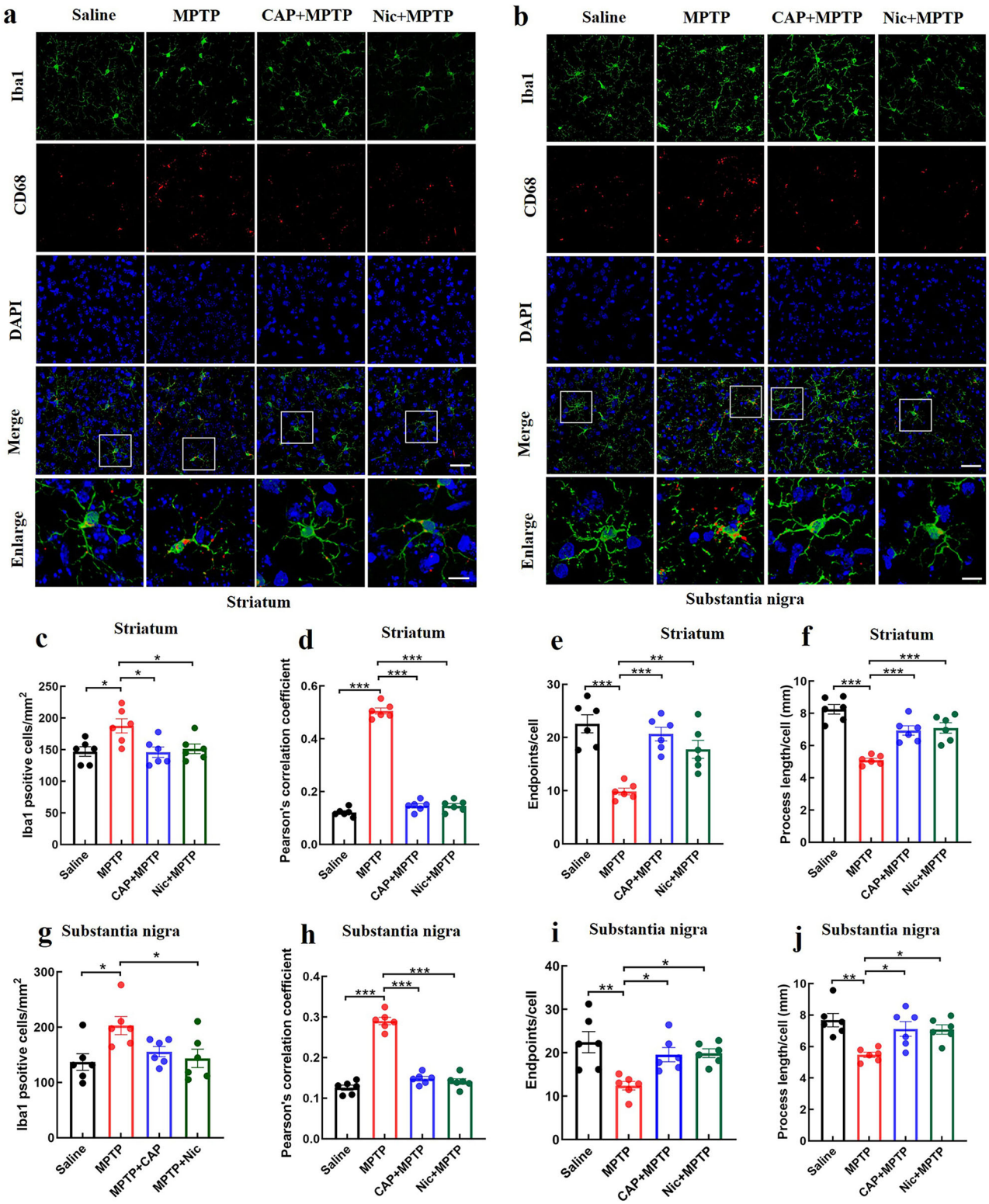

Fig. 7 | Effects of CAP and Nic on microglia in the striatum and substantia nigra of MPTP-induced mice. **a** Representative immunofluorescence images of Iba1 and CD68 in the striatum; **b** Representative immunofluorescence images of Iba1 and CD68 in the substantia nigra; **c** Iba1 positive cells in the striatum; **d** Iba1 and CD68 co-localization in the striatum; **e** Iba1 endpoints in the striatum; **f** Iba1 process length in the striatum; **g** Iba1 positive cells in the substantia nigra; **h** Iba1 and CD68 co-localization in the substantia nigra; **i** Iba1 endpoints in the substantia nigra; **j** Iba1 process length in the substantia nigra. Iba1: green; CD68: red; DAPI: blue; Images were captured using a 63× objective, scale bar = 25 μm; enlarge scale bar = 2.5 μm. ($n = 6$ mice per group for **a**–**j**). Statistical analyses were performed by one-way ANOVA followed by Tukey's multiple comparison test. $^{*}p < 0.05$, $^{**}p < 0.01$, $^{***}p < 0.001$.

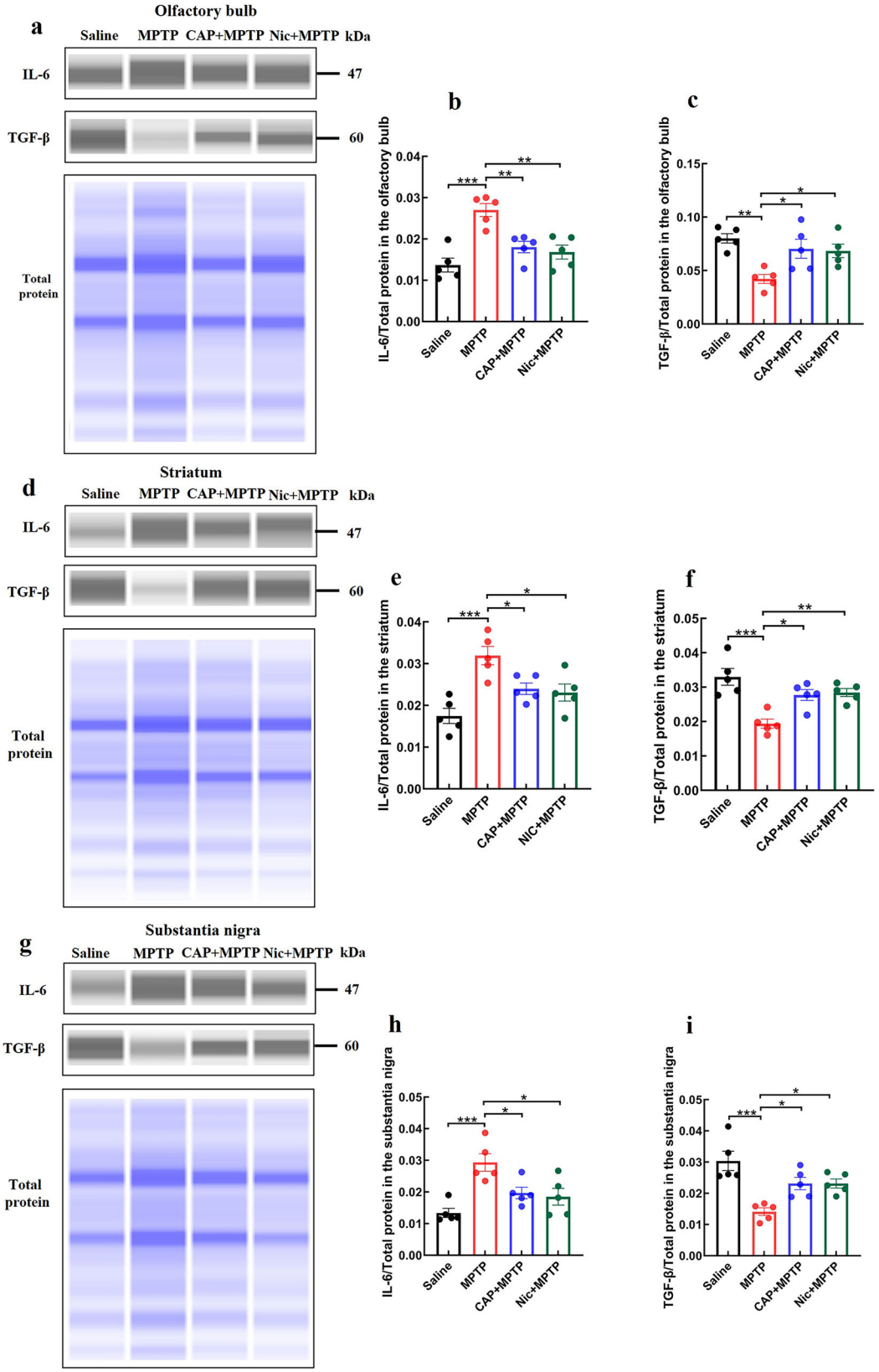

Fig. 8 | Effects of CAP and Nic on IL-6 and TGF-β expression in MPTP-induced mice. a Representative automated western immunoblotting images of IL-6 and TGF-β in the olfactory bulb; **b** The IL-6 statistical results in the olfactory bulb; **c** The TGF-β statistical results in the olfactory bulb; **d** Representative automated western immunoblotting images of IL-6 and TGF-β in the striatum; **e** The IL-6 statistical results in the striatum; **f** The TGF-β statistical results in the striatum; **g** Representative automated western immunoblotting of IL-6 and TGF-β in the substantia nigra; **h** The IL-6 statistical results in the substantia nigra; **i** The TGF-β statistical results in the substantia nigra. ($n = 5$ mice per group for **a**–**i**). Statistical analyses were performed by one-way ANOVA followed by Tukey's multiple comparison test. $^{*}p < 0.05$, $^{**}p < 0.01$, $^{***}p < 0.001$.

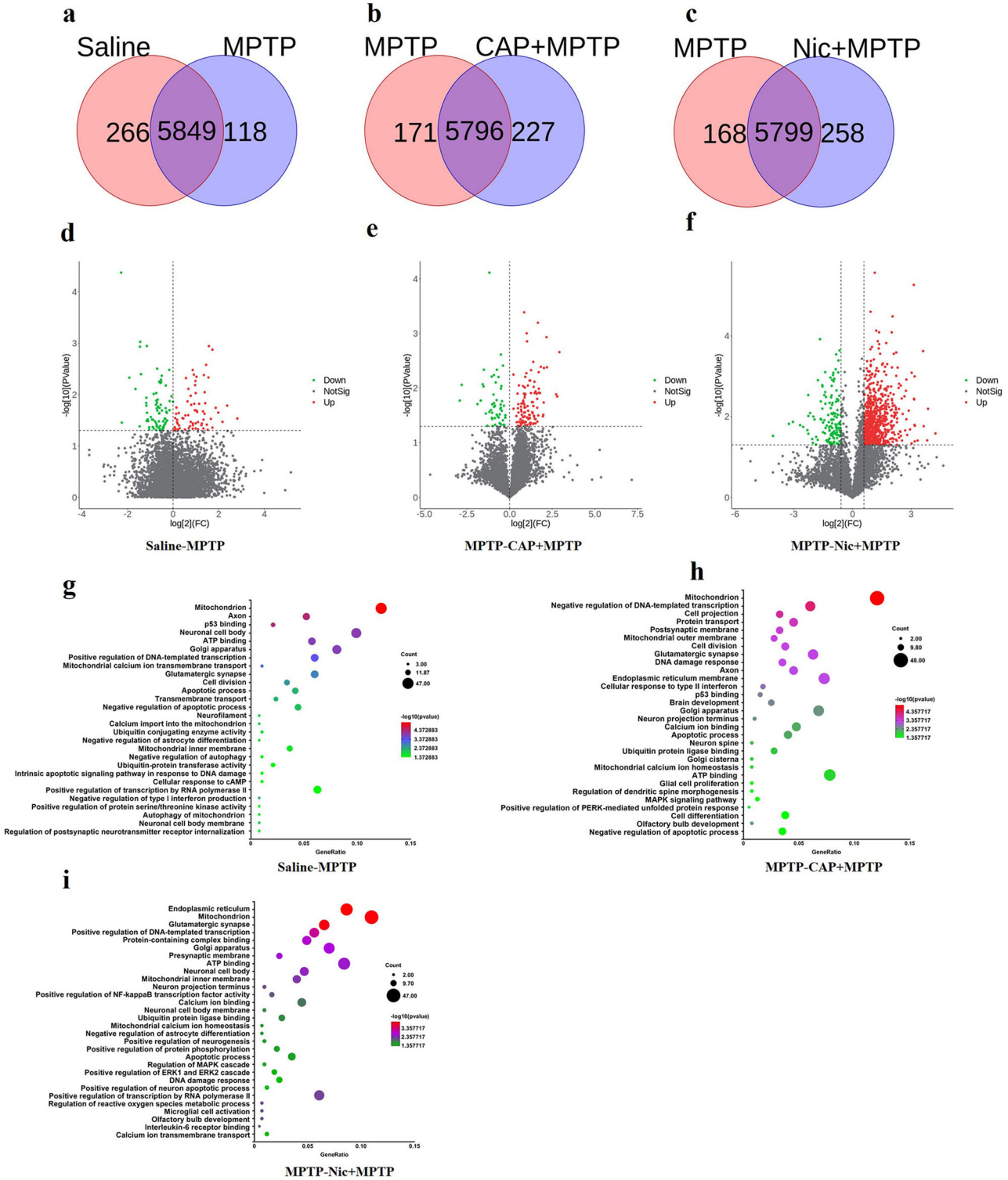

Fig. 9 | Proteomics analysis in the olfactory bulb of MPTP-induced mice. Venn diagram of protein: **a** saline and MPTP samples; **b** MPTP and CAP + MPTP samples; **c** MPTP and Nic+MPTP samples. Volcano plots showed the results of differentially expressed protein in **d** saline and MPTP samples; **e** MPTP and CAP + MPTP samples; **f** MPTP and Nic+MPTP samples; (|log 1.5 (FoldChange)| > 1 & padj< 0.05). Analysis of GO pathways enriched with differentially expressed protein in (**g**) saline and MPTP samples; **h** MPTP and CAP + MPTP samples; **i** MPTP and Nic+MPTP samples; ($n = 3$ mice per group for **a**–**i**).

role in the neuroprotective regulatory mechanisms of CAP and Nic. Additionally, the meta-analysis revealed that significantly differentially expressed genes (including *ISG15* and *IRF-7*) are regulated via the TBK1 pathway. KEGG/GO enrichment analysis of proteomics data further implicated TBK1 in mitochondrial and autophagic processes, and indicated a close connection between TBK1 and the cGAS-STING signaling axis. Concurrently, transcriptomics enrichment analysis showed that the DNA damage response pathway converges at the cGAS/TBK1/STING hub. Based on these findings, we further investigated whether CAP and Nic exert neuroprotective effects in the PD model with olfactory dysfunction by modulating the cGAS/TBK1/STING signaling pathway. These findings indicate that CAP and Nic may exert neuroprotective effects in the MPTP-

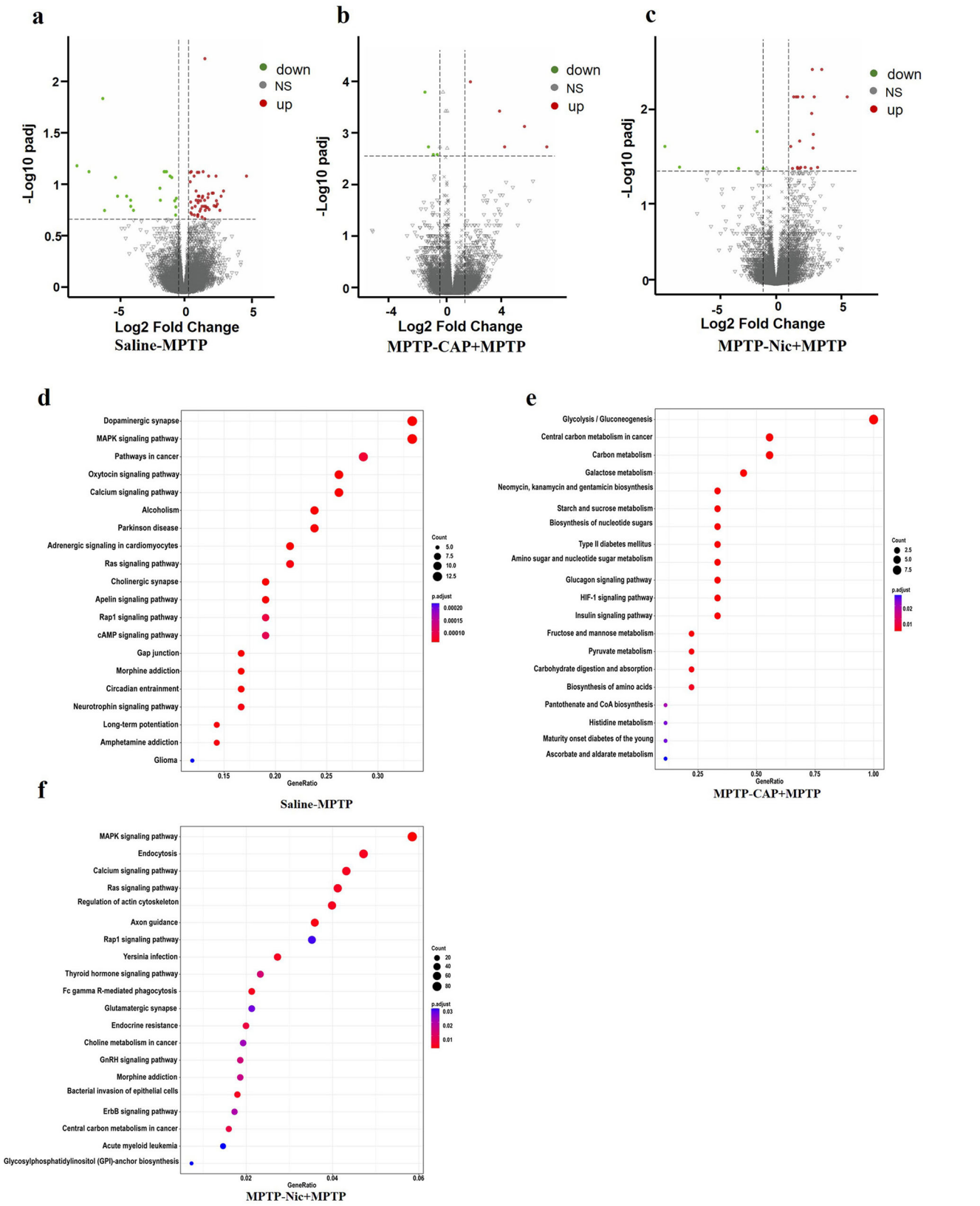

Fig. 10 | Transcriptomic analysis in the olfactory bulb of MPTP-induced mice. Volcano plots showed the results of differentially expressed genes in **a** saline and MPTP samples; **b** MPTP and CAP + MPTP samples; **c** MPTP and Nic+MPTP samples; (|log 2 (FoldChange)| > 1 & padj< 0.05). Analysis of KEGG pathways enriched with differentially expressed genes in **d** saline and MPTP samples; **e** MPTP and CAP + MPTP samples; **f** MPTP and Nic+MPTP samples. ($n = 3$ mice per group for **a**–**f**).

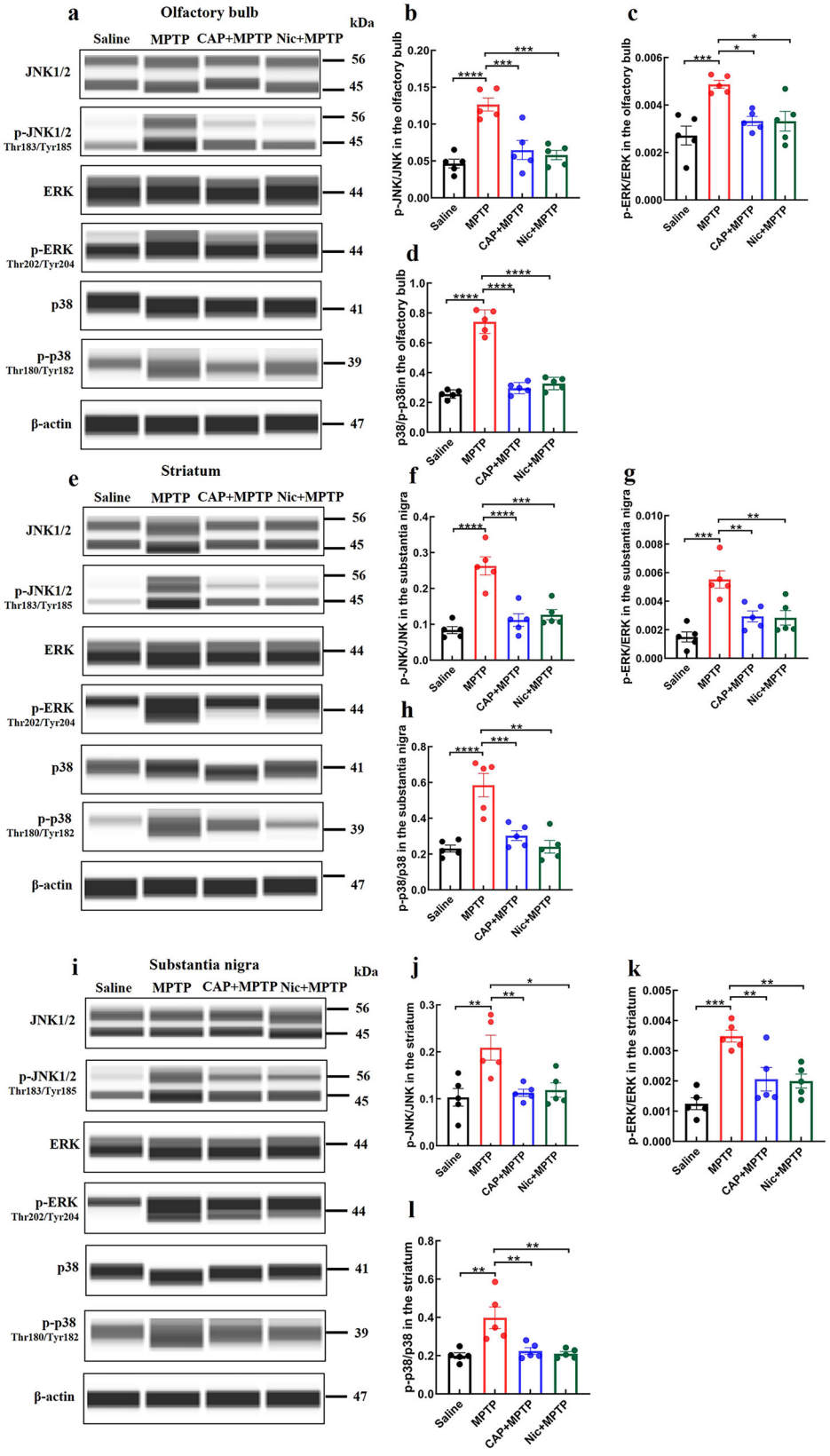

Fig. 11 | Effects of CAP and Nic on the MAPK signaling pathway in MPTP-induced mice. **a** Representative automated western immunoblotting images of the MAPK signaling pathway in the olfactory bulb; **b** The p-JNK/JNK statistical results in the olfactory bulb; **c** The p-ERK/ERK statistical results in the olfactory bulb; **d** The p-p38/p38 statistical results in the olfactory bulb; **e** Representative automated western immunoblotting images of the MAPK signaling pathway in the striatum; **f** The p-JNK/JNK statistical results in the striatum; **g** The p-ERK/ERK statistical results in the striatum; **h** The p-p38/p38 statistical results in the striatum; **i** Representative automated western immunoblotting images of the MAPK signaling pathway in the substantia nigra; **j** The p-JNK/JNK statistical results in the substantia nigra; **k** The p-ERK/ERK statistical results in the substantia nigra; **l** The p-p38/p38 statistical results in the substantia nigra. ($n = 5$ mice per group for **a**–**l**). Statistical analyses were performed by one-way ANOVA followed by Tukey's multiple comparison test. $^{*}p < 0.5$, $^{**}p < 0.01$, $^{***}p < 0.001$, $^{****}p < 0.0001$.

induced olfactory dysfunction mouse model by modulating the MAPK/cGAS-STING signaling pathways. Transcriptomic inter-sample correlation analysis, striatum and substantia nigra regions differential gene expression, and olfactory bulb GO enrichment analysis are shown in the figure (Supplementary Information Fig. 3).

Capsaicin and nicotine intervention inhibit MPTP-induced activation of the MAPK signaling pathway

The MAPK signaling pathway is involved in various disease-related pathological processes, such as oxidative stress, neuroinflammation, autophagy, and neuronal death. Abnormal activation of the MAPK

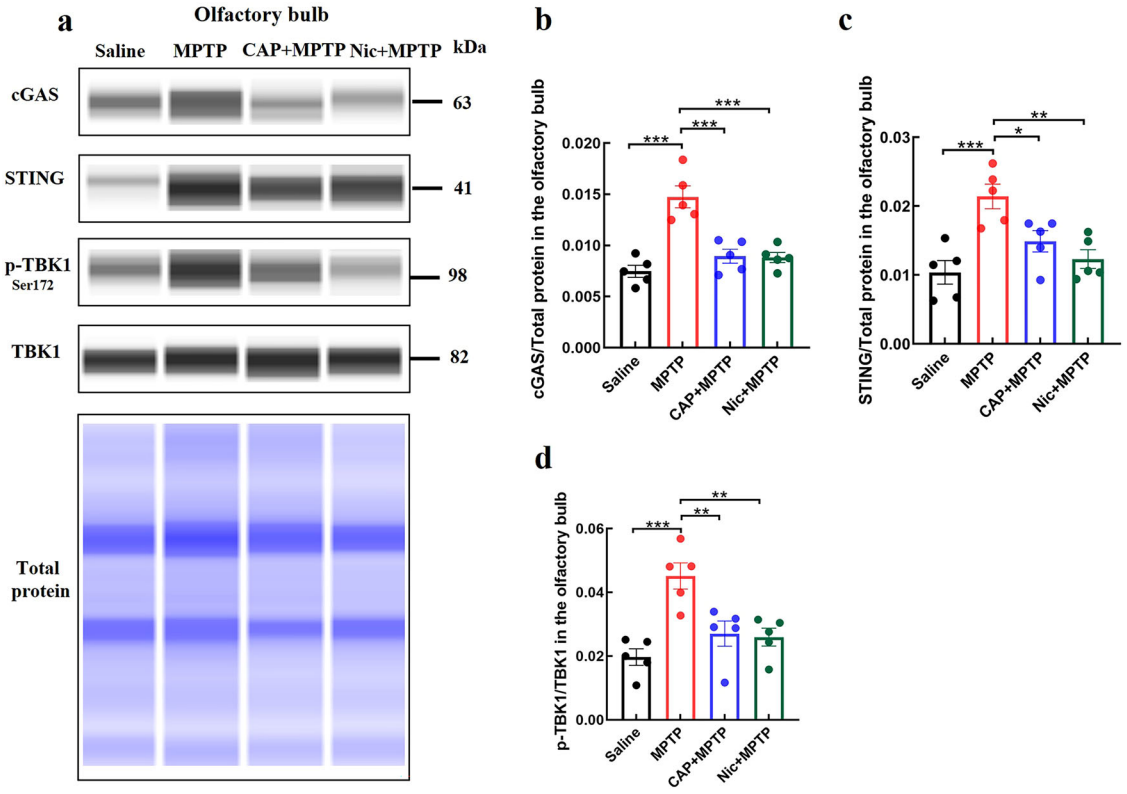

Fig. 12 | Effects of CAP and Nic on the cGAS-STING signaling pathway in the olfactory bulb of MPTP-induced mice. a Representative automated western immunoblotting images of the cGAS-STING signaling pathway in the olfactory bulb; **b** The cGAS statistical results in the olfactory bulb; **c** The p-TBK1/TBK1 statistical results in the olfactory bulb; **d** The STING statistical results in the olfactory bulb; ($n = 5$ mice per group for **a**–**d**). Statistical analyses were performed by one-way ANOVA followed by Tukey's multiple comparison test. $^{*}p < 0.5$, $^{**}p < 0.01$, $^{***}p < 0.001$.

signaling pathway may lead to dopaminergic neuronal apoptosis and exacerbate neuroinflammatory responses[48]. To investigate whether the neuroprotective effects of CAP and Nic intervention are mediated through the regulation of the MAPK signaling pathway, the Jess™ analysis system was used to analyze the expression levels of key proteins in the three major branches of the MAPK pathway: the JNK pathway (p-JNK and total JNK), the ERK pathway (p-ERK and total ERK), and the p38 pathway (p-p38 and total p38). First, the expression of the MAPK pathway in the olfactory bulb, striatum and substantia nigra regions were examined. The results (Fig.11a-l) showed that, compared to the saline group, the ratios of p-JNK/JNK, p-ERK/ERK, and p-p38/p38 were significantly increased in the MPTP group. However, the CAP + MPTP and Nic+MPTP groups exhibited significantly reduced ratios of p-JNK/JNK, p-ERK/ERK, and p-p38/p38 compared to the MPTP group. These findings indicate that CAP and Nic intervention can suppress the MAPK signaling pathway in the olfactory bulb, striatum and substantia nigra regions of PD mice. (Uncropped and unprocessed blot scans in the Supplementary Information).

Capsaicin and nicotine intervention inhibit MPTP-induced activation of the cGAS-STING signaling pathway

The cGAS-STING pathway is closely associated with DNA damage and mitochondrial dysfunction[49], and STING deficiency in a chronic mitochondrial stress mouse model has been shown to rescue motor deficits and the loss of dopaminergic neurons[50]. This finding prompted us to further investigate whether CAP and Nic exert the neuromodulatory effects through the cGAS-STING signaling pathway. The results (Fig. 12a–d) showed that, using the Jess™ analysis system, the expression levels of cGAS, STING, p-TBK1, and TBK1 proteins in the olfactory bulb, striatum and substantia nigra regions were assessed. Compared to the saline group, the MPTP group exhibited significantly increased expression levels of cGAS, STING, and p-TBK1/TBK1. In contrast, the CAP + MPTP and Nic +MPTP groups showed significantly reduced expression levels of STING and p-TBK1/TBK1 compared to the MPTP group. These findings indicate that CAP and Nic intervention can suppress the cyclic GMP-AMP synthase/stimulator of interferon genes (cGAS/STING) signaling pathway in the olfactory bulb of PD mice.However, no significant changes were observed in cGAS-STING signaling pathway protein expression in the striatum and substantia nigra regions are shown in the figure (Supplementary Information Fig. 4 and uncropped and unprocessed blot scans in the Supplementary Information).

Discussion

A single intranasal administration of MPTP to C57BL/6 mice recapitulates early-stage PD pathology, characterized by olfactory dysfunction and dopaminergic neuronal damage in the striatum and substantia nigra[11]. Studies in rat models also confirm that intranasal MPTP administration induces deficits in olfactory discrimination and social recognition. This neurotoxin gains direct access to the brain via the olfactory mucosa, subsequently disrupting dopaminergic function across multiple brain structures[51]. These findings demonstrate that intranasal MPTP delivery establishes a valid PD model with olfactory impairment. Subcutaneous MPTP injection in C57BL/6 J mice reliably induces olfactory deficits, while methylene blue gavage significantly ameliorates MPTP-induced olfactory dysfunction, motor coordination impairments, and degeneration of TH neurons in the striatal-nigral pathway[52]. Intraperitoneal MPTP administration compromises olfactory discrimination and detection capabilities in mice. Nic intervention restores cholinergic neuronal projections from the horizontal limb of the diagonal band (HDB) to the olfactory bulb and dopaminergic innervation, thereby improving cholinergic system dysfunction[53]. Collectively, these studies confirm that pharmacological interventions can effectively mitigate MPTP-induced olfactory deficits in PD models. Building on this evidence, we established a PD mice model via

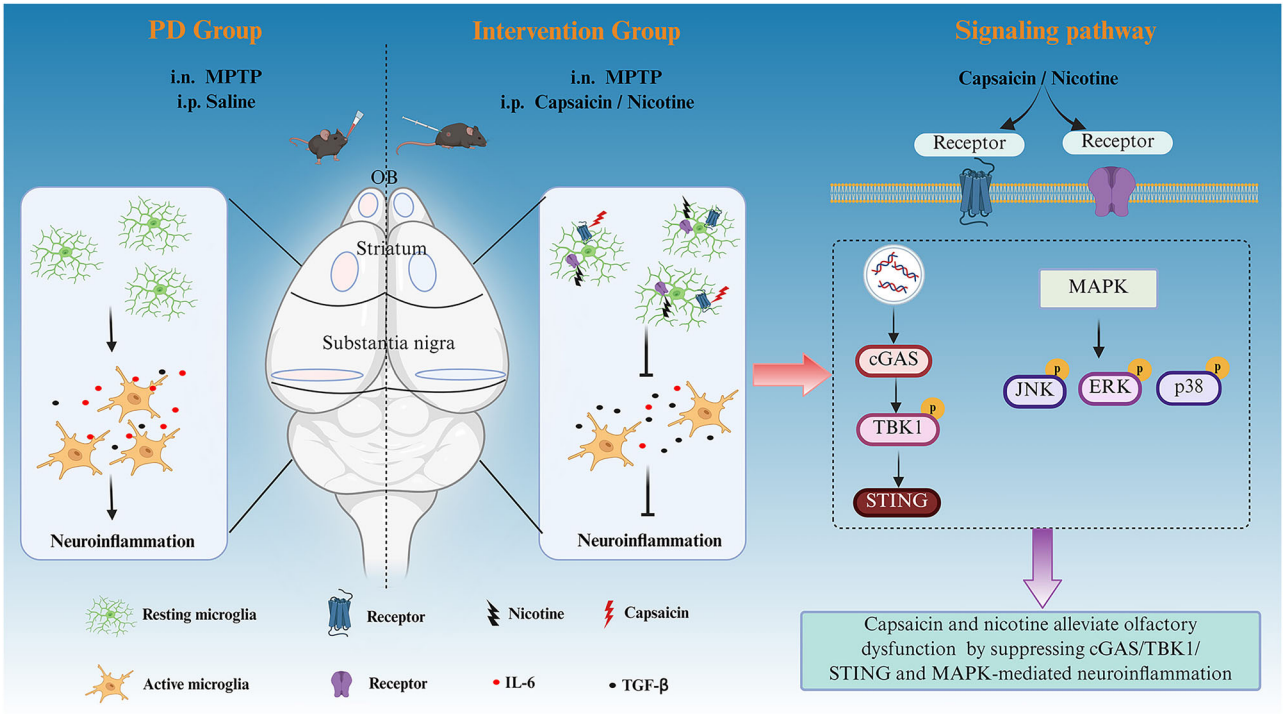

Fig. 13 | Schematic summary of the mechanism underlying the neuroprotective actions of CAP and Nic in PD. Created in BioRender. https://BioRender.com/weby68u.

intranasal MPTP administration and investigated the neuroprotective mechanisms of CAP and Nic against olfactory dysfunction at the molecular level.

Olfactory and motor behavioral tests demonstrated that intranasal MPTP successfully induced olfactory dysfunction in mice, and CAP and Nic intervention can effectively alleviate olfactory dysfunction, anxiety, and motor deficits in PD mice.Pathological experiments revealed that intervention with CAP and Nic reduced dopaminergic neuronal damage in the olfactory bulb, olfactory tubercle, striatum, and substantia nigra regions of PD mice with olfactory dysfunction, inhibited microglial activation, and modulated the expression of inflammatory factors IL-6 and TGF-β. Further integrated transcriptomic and proteomic analyses suggest that CAP and Nic may alleviate olfactory dysfunction in PD mice by inhibiting the MAPK and cGAS-STING signaling pathways (Fig. 13).

PD is a neurodegenerative disorder characterized primarily by the progressive loss of dopaminergic neurons in the SNc. Non-motor symptoms, particularly olfactory dysfunction, have garnered significant attention as important biological markers in the prodromal phase of PD[54]. Olfactory impairment is closely associated with Lewy body deposition and neurotransmitter degeneration. As a key biological marker for early diagnosis of PD, olfactory dysfunction not only provides a crucial basis for early disease identification but also opens new avenues for exploring the pathological mechanisms of PD and developing neuroprotective strategies, which are of significant clinical importance in slowing disease progression.

Research indicates that CAP has neuroprotective effects on PD[55]. Epidemiological studies have found a lower incidence of PD among smokers[56]. Both CAP and Nic have been shown to ameliorate dopaminergic neuron damage. Numerous studies suggest that CAP can inhibits activate microglia, reduce the production of reactive oxygen species (ROS), and thereby inhibit the secretion of pro-inflammatory factors. Additionally, CAP can increase dopamine levels and reduce oxidative stress, indicating its potential neuroprotective role in PD[55,57]. These effects can improve motor symptoms and alleviate dopaminergic neuron damage, potentially preventing PD. Nic, a natural agonist of nAChRs, has been shown to exacerbate PD pathology in mice due to nAChR deficiency. Nic can activate M1-type microglia to reduce the secretion of pro-inflammatory cytokines from peripheral macrophages, thereby improving dopaminergic neuron imbalance and exerting a neuroprotective effect in PD[58]. Nic also alleviates motor deficits in α-Syn PD models and exerts neuroprotective effects by modulating α4 β2 and α7 nAChRs[59].

According to the Braak staging hypothesis, abnormal α-Syn first appears in the olfactory bulb. Other regions of the olfactory system, such as the anterior olfactory nucleus, cortical amygdala, piriform cortex, olfactory tubercle, entorhinal cortex, and orbitofrontal cortex, also show LBs deposition[60]. The loss of dopaminergic neurons in the substantia nigra leads to dopamine deficiency in the striatum[61], resulting in PD motor symptoms. Pathological changes in these regions are closely related to olfactory and motor dysfunction in PD. Dopaminergic neurons play a crucial role in the pathogenesis of PD[62]. The nigrostriatal pathway, which contains the highest concentration of dopaminergic neurons, can lead to PD when dopamine DA function declines due to self-regulation or external stimuli[63]. Dopaminergic neurons also innervate several structures of the olfactory system[64], such as the olfactory tubercle, entorhinal cortex, and piriform cortex, primarily regulating cognitive and perceptual abilities in the mesolimbic and mesocortical pathways. The glomerular layer of the olfactory bulb contains approximately 10% dopaminergic interneurons, which are involved in olfactory processing and determine olfactory ability. Dopaminergic neuron receptors are expressed in the olfactory bulb[62,65]. Dopaminergic neurons are considered highly plastic in olfactory pathway operation[66]. However, olfaction has not been found to respond to dopaminergic replacement therapy. It remains unclear whether changes in dopaminergic neuron levels are directly related to hyposmia or if there is a common underlying mechanism. In this study, we found that CAP and Nic interventions could alleviate dopaminergic neuron damage in the olfactory bulb, olfactory tubercle, striatum, and substantia nigra regions in MPTP-induced PD mice.

Evidence suggests that the olfactory bulb may be particularly susceptible to inflammation-related pathology, especially inflammation triggered by microglia[67]. Integrated proteomics and transcriptomics studies revealed concordant dysregulation in MAPK signaling, axon, cell projection, ATP binding, dopaminergic synapse and PD processes, substantiating their synergistic roles in MPTP-induced mice pathology. We conducted pathway analysis of the MAPK and cGAS/TBK1/STING signaling axes to further

elucidate the neuroprotective mechanisms of CAP and Nic in PD mice with olfactory dysfunction. In MPTP-treated mice, the activation of the JNK signaling pathway, which involves c-Jun phosphorylation, is associated with the induction of apoptosis[68,69]. ERK1/2 has been shown to promote cell death in both in vitro and in vivo neuronal death models[70]. p38 MAPK is activated in PD models and is associated with neuronal cell death mechanisms[71,72]. The STING pathway can regulate cellular metabolism, improve neuronal energy supply, inhibit neuroinflammation, and promote neural development and myelination. TBK1, a serine/threonine protein kinase, regulates antiviral defense, host-virus interactions, and the suppression of inflammation[73]. Activation of the cGAS-STING pathway can modulate microglia, promote neuroinflammation, and lead to neuronal cell death[74]. Research suggests that α-Syn aggregates can increase STING expression and enhance STING activation, indicating that elevated STING levels may lead to increased neuroinflammation and neuronal cell damage or death. Therefore, inhibiting STING may have therapeutic potential for diseases like PD caused by α-Syn aggregates[75]. This study found that inhibiting the MAPK/cGAS-STING signaling pathway could alleviate olfactory dysfunction in MPTP-induced PD mice.

In summary, this study thoroughly investigated the neuroprotective effects and underlying mechanisms of CAP and Nic in PD mice with olfactory dysfunction. The results demonstrated that CAP and Nic likely regulate microglia-mediated inflammatory responses through the cGAS-STING and MAPK signaling pathways, significantly reducing IL-6 while increasing TGF-β and other inflammatory cytokine expression levels. This consequently alleviates dopaminergic neuron damage in key brain regions of PD mice with olfactory dysfunction, including the olfactory bulb, olfactory tubercle, striatum, and substantia nigra regions. Furthermore, CAP and Nic intervention also showed improvement in motor dysfunction in PD mice. These findings not only reveal the potential therapeutic value of CAP and Nic in treating PD-related olfactory disorders but also provide an important experimental foundation for further exploration of their molecular mechanisms and clinical translation research.

Methods

Experimental animals

C57BL/6 mice, 6–8 weeks and weighing 18-20 g, were provided by Beijing Huafukang Bioscience Co., Ltd. (License No.: SCXK (Jing) 20190008, Beijing, China). Female mice were selected in this study because many studies have shown that females exhibit superior performance in tests of odor identification[76–78]. The mice were housed under controlled temperature and humidity conditions (22 ± 1°C) with a 12-hour light/dark cycle, and provided with feed and water to ensure free access to food and drinking. The animal trials were conducted following the guidelines of the National Institute of Health for the Care and Utilization of Laboratory Animals and were authorized by the Ethics Review Committee of Life Sciences at Zhengzhou University, ensuring that all animal experiments complied with regulatory requirements.

Buried pellet test

The block test was conducted as previously described[79]. The mice ability to detect odors were assessed through buried pellet test. At least two days before testing, the weight of each mouse were recorded and then food restriction to 90% of mice body weight were performed. Prior to the buried pellet testing and during food restriction, 1-2 pieces of the pellets to be used during the test were given to each mouse (e.g., a piece of sweetened cereal). On the test day, habituate the mice for 1 hour prior to testing by placing their cage in the testing room with no water bottle or feeder bin. House the mice in their home cage with just a filter top lid and bury a piece of the pellet 0.5 cm below the bedding. In each trial, the mouse was placed at the center of the cage at the beginning. When the pellet was detected and eaten by mouse, the timer stopped and the time was recorded. If the mouse did not find the pellet in 5 min, the test stopped and a score of 300 seconds was noted for it. The bedding in the test chamber was cleaned for each trial. The pellet was buried in a different spot in the cage between trials. The researcher changed gloves between each trial so that the scents were not exchanged between animals while residual odors were removed by cleaning with 70% ethanol.

Block test

The block test was conducted as previously described[79]. To assess the ability of mouse to discriminate the social scent, a block test was used. To take the odor of mice respectively, each wooden block (2 cm× 2 cm×2 cm) was sealed in a plastic bag with 8 g of animal beddings from the home cages of tested mice for 24 h. One block carried the own odor of the mouse, while the other four blocks carried the odor of an unfamiliar mouse in each trial, then the test mice were moved to the testing area that was with five kinds of wooden blocks of different odor (one block with its own odor, another ones with the odor of unfamiliar mouse). Then the test mouse could smell the two kinds of wooden blocks of different odor. The timer was used to record the time for every mouse sniffed the novel odor (unfamiliar mouse) and the self-odor in a 180 s trail. The sniffing time for the novel odor and the self-odor was calculated and analyzed. Meanwhile, the relative ratio of sniffing time of novel scent to own scent (novel scent/own scent) was calculated and analyzed. The researcher changed gloves between each trial so that the scents were not exchanged between the blocks and residual odors were removed by cleaning with 70% ethanol.

Olfactory preference and avoidance test

The olfactory preference and avoidance test was conducted as previously described[5]. The ability of mouse to perceive and discriminate the social scent was assessed through the olfactory preference and avoidance test. The mice were placed in a test cage measuring 36 cm (width) × 24.5 cm (depth) × 15 cm (height). Two pieces of filter paper (2 cm × 2 cm) were positioned at the bottom of the cage, 8.5 cm from the long side and 6.5 cm from each short side.

For the olfactory preference test, a test odorant (mouse urine) was applied to the filter paper on one side of the cage, while water was applied to the filter paper on the opposite side. The timer was used to record the time for every mouse sniffed the mouse urine and the water in a 180 s trail.

For the olfactory avoidance test, a bisector was introduced into the cage, and two pieces of filter paper were placed on opposite sides. A test odorant (hexanone) was applied to the filter paper on one side, and water was applied to the filter paper on the opposite side. The timer was used to record duration of time for every mouse stay in each of the two odor zones in a 180 s trail.

Olfactory behavior training system

The olfactory behavior training system was conducted as previously described[80]. The olfactory training system go/no-go (RWD Olfactometer OM-16, China) was used to assess the comprehensive abilities in odor detection, discrimination, learning, and memory. At least two days before testing, the mice were water restricted to maintain approximately 85% of their body weight, ensuring they had a strong desire to drink water prior to the experiment. The behavioral training process consisted of three stages: mode licking teaching, mode odor related, and go/no-go. In the mode licking teaching stage, the mice were head-fixed in the behavioral setup and trained to voluntarily lick water delivered from a water spout, with each mouse undergoing 100 trials per day for 2-3 days until they learned to voluntarily lick the water. In the mode odor related stage, the mice were trained to associate the water reward with the odor of isoamyl acetate, which involved two phases: phase A, where the odor was presented for 1 second and water was actively delivered with a 0.5-second response time, and phase B, where the mice had to actively lick the spout upon detecting the odor to receive water. Each session consisted of 20 trials, and the mice were trained for 5 sessions (100 trials) per day for 2-3 days, proceeding to the next stage once they achieved a correct response rate of over 80% in two consecutive sessions. In the go/no-go stage, two odors were introduced: isoamyl acetate and heptanone, with the mice required to lick the spout within 0.5 seconds upon detecting isoamyl acetate (recorded as a hit) or refrain from licking upon detecting heptanone (recorded as a correct rejection). Failures to lick

after detecting isoamyl acetate were recorded as misses, while licks after detecting heptanone were recorded as false choices. Each session consisted of 20 trials, and each mouse was trained for 5 sessions (100 trials) per day for 3 consecutive days, with 10-15 min of free access to water provided after each session and 70% anhydrous ethanol used to eliminate any residual odors left by the mice. This training protocol was designed to evaluate the ability to associate odors with rewards and their decision-making accuracy in response to different olfactory cues.

Open field test

The open field was divided into 16 small squares of 4×4 on the bottom, with a camera mounted directly above to cover the entire open field area. During the test, every mouse was first placed in the center of a 45 cm × 45 cm × 45 cm open field box and allowed to move freely for 1 minute. The computer tracking system (developed by Xinruan Information Technology Co., Ltd., China) was then used to analyze the mouse's activity status over a period of 5 min. The trajectory map of the mice were obtained to measure their motor abilities, and the distance and time spent in the central and peripheral areas were used to assess the anxiety levels of the experimental animals. Before each trial, 70% anhydrous ethanol was used to eliminate any residual scent left by the mice.

Rotarod test

The rotarod test (Xinruan Information Technology Co., Ltd., China) was conducted to assess the motor coordination ability. On the day before the experiment, the mice were placed on the rotarod at a constant speed of 10 r/min for 20 min to acclimate them to the new environment and the mode of movement. On the following day, the mice were placed on the rotarod device with accelerating rotation. Over a period of 6 min, the speed gradually increased from 5 r/min to 40 r/min. The time from the start of the rotation until the mouse fell off the rotarod was recorded. Each animal was tested three times, with a 5 min interval between trials, and the average value of the three trials was calculated. The rotarod test was used to evaluate the motor abilities of the mice. Before each trial, 70% anhydrous ethanol was used to eliminate any residual odors left by the mice.

Immunohistochemistry

Mice were euthanized and perfused with saline and then ice-cold 4% paraformaldehyde. Subsequently, remove the mouse brain tissue and dehydrate it sequentially in 4% paraformaldehyde solution, 10% sucrose, 20% sucrose, and 30% sucrose solutions and cut into 25 μm slices by machine of frozen slicer (Leica, Germany). For immunohistochemistry coronal sections of the mouse brain were incubated with 3% H_2O_2 at room temperature for 25 min to inactivate endogenous enzymes and were blocked with 10% bovine serum albumin (BSA) in buffered saline 0.1 M PBS (pH 7.4) for 1 h at room temperature. Tyrosine hydroxylase (1:1000, AB152, Millpore, USA)-positive neurons in the olfactory bulb, olfactory tubercle, striatum and substantia nigra regions were identified through immunohistochemistry using the SABC (rabbit IgG) - POD Kit (SA0021, Solarbio, China). The images were obtained by a confocal microscope (Motic Easy Scan, China) and quantifications were performed by the software Image J (version 2.1.0).

Immunofluorescence

Coronal sections of the mouse brain were blocked with 10% BSA in PBS for 2 h at room temperature. Afterward, the samples were incubated with following primary antibodies for 14 h: anti-Iba1 (1:1000, 019-19741, Wako, Japan) and anti-CD68 (1:1000, 137001, BioLegend, China). The samples were incubated with the following secondary antibodies for 2 h in the dark: Alexa fluor 488-conjugated anti-rat immunoglobulin IgG (1:200, ZF-0318, ZSGB-BIO, China) and alexa fluor 568-conjugated anti-rabbit IgG (1:200, ZF0311, ZSGB-BIO, China). Finally, the sections were mounted and sealed with an anti-fade mounting medium containing DAPI (0100-20, SouthernBiotech, USA). Images were acquired using a Leica TCS SP8 confocal microscope (Leica, Germany).

Jess™ Automated Western Immunoblotting

The olfactory bulb, striatum, and substantia nigra tissues were quickly removed from the mice brain after anesthesia execution and homogenized in RIPA lysis buffer (200 μL, R0010, Solarbio, China), Protease inhibitor cocktail (2.04 μL, HY-K0022, MCE, USA), Phosphatase inhibitor cocktail II (2.02 μL, HY-K0022, MCE, USA), PMSF (2 μL, P0100, Solarbio, China). The protein concentration is then determined using the BCA protein assay kit (PC0020, Solarbio, China). As previously reported in our study[81,82], the Jess™ Simple Western (ProteinSimple, USA) along with the Separation Module (SM-W004, ProteinSimple, USA), while detection was performed using the Antibody Detection Module (DM-001, ProteinSimple, USA). In this experiment, total protein normalization (TPN) was employed to normalize the abundance of target proteins to the total protein content in each sample. Prepare DTT, 5×Master Mix, and Ladder solutions separately, then add the tissue proteins and denature at 95 °C for 5 min, followed by cooling on ice for 5 min. After cooling, vortex mixing and briefly centrifuge. Subsequently, dilute the primary antibody, prepare the luminescent solution Lumino-S and Peroxide(1:1), prepare the total protein reagent 1 and total protein reagent 2 (DM-TP01, ProteinSimple, USA), and the elution buffer RePlex™ reagent 1 and RePlex™ reagent 2 (RP-001, ProteinSimple, USA), and mix well and keep on ice for later use. Add the reagents to the corresponding wells in the reagent plate according to the instructions.

Sample preparation for transcriptomics

The olfactory bulb, striatum, and substantia nigra tissues were cut into small pieces for total mRNA extraction, which was subsequently used for transcriptomic sequencing. Transcriptional RNA sequencing was performed by the Wekemo Bioincloud Corporation (Shenzhen, China). Analysis was performed using the Bioincloud (https://www.bioincloud.tech/) bioinformatics cloud platform.

Transcriptomics bioinformatics

The raw data underwent quality control processing using FastQC (version 0.23.1) to facilitate subsequent analysis. The quality-controlled Clean data reads were then aligned to the reference genome using Hisat2 (version 2.2.1) in preparation for downstream assembly. Variant calling analysis was performed on the aligned data of each sample using GATK (version 4.2.2.0). RNA-Seq data were utilized for alternative splicing analysis, and the rMATS software (version 4.1.1) was employed to quantify and analyze differential alternative splicing events. The data were subsequently normalized, and the Benjamini-Hochberg correction (BH) was applied to obtain adjusted *p*-values. Differential gene expression analysis was conducted using DESeq2 (version 1.26.0), with a significance threshold set at padj < 0.05. Finally, the ClusterProfiler software (version 3.14.3) was used to perform KEGG and GO pathway enrichment analysis on the differentially expressed genes Analysis was performed using the Bioincloud (https://www.bioincloud.tech/) bioinformatics cloud platform.

Sample preparation for proteomics

Protein extraction from olfactory bulb tissues was performed using the EasyPept Micro-48X (OSFP0001, Omicsolution, China) with 200 μL ice-cold lysis buffer (supplemented with protease/phosphatase inhibitors) per 25 mg tissue. Following homogenization via a high-throughput tissue grinder, samples were denatured at 95 °C for 5 min in a metal heat block and centrifuged at 12000 × g and 4 °C for 30 min. The supernatant was collected. Reagent A was added and mixed by pipetting, incubated at 95 °C for 5 min, cooled to room temperature, then treated with 15 μL Reagent B for 2 h. Digestion was terminated by adding Reagent C. After centrifugation at 20,000 × g the digest was desalted using spin columns pre-activated and equilibrated per manufacturer's protocol. Samples were loaded onto columns (700 × g, 1 min), washed with 100 μL Wash Buffer (700 × g, 1 min), and eluted with 50 μL Elution Buffer. Eluates were concentrated by vacuum centrifugation, stored at -80 °C, and reconstituted in 1% formic acid prior to Liquid Chromatography-Tandem Mass Spectrometry (LC-MS/MS) analysis.

Liquid chromatographic data acquisition

Data acquisition was performed using an Orbitrap Eclipse™ Tribrid™ (ThermoFisher, USA) MS coupled with an EASY-nLC 1000 LC (ThermoFisher, USA) system. The chromatographic separation system consisted of a trap column (Acclaim™ PepMap™ C18, 3 μm, 75 μm × 2 cm) and an analytical column (Acclaim™ PepMap™ C18, 1.9 μm, 100 Å, 75 μm × 15 cm). Peptide separation was carried out at a flow rate of 300 nL/min with a total run time of 75 min as detailed in Supplementary Information Table 1. The mobile phase composition was as follows: mobile phase A was an aqueous solution containing 0.1% formic acid, and mobile phase B was an aqueous solution containing 0.1% formic acid and 80% acetonitrile.

Mass spectrometry data acquisition

For peptide analysis, MS data acquisition was performed using a 75 minute liquid LC-MS method with positive-polarity detection and high-resolution Orbitrap-based analysis. The ion source was configured with high-field asymmetric waveform ion mobility spectrometry (FAIMS) in standard resolution mode, maintaining a carrier gas flow of 3.8 L/min (static mode) and setting the FAIMS compensation voltage (CV) at -40 V. For the MS OT (master scan-Orbitrap), an Orbitrap detector with a resolution of 240,000 was used, covering a mass range of 375–1500 m/z. The RF lens was set to 40%, the automatic gain control (AGC) target was standardized at an absolute value of 4.000×10^5, the maximum injection time was 502 ms, and only 1 microscan was performed per acquisition. The [FAIMS-40v] experiment ran from 0 to 75 min with a 2 seconds cycle time, operating in cycle time-based data-dependent mode (2 seconds interval between master scans). During the scan event (ddMS² OT HCD), quadrupole isolation was applied with a 1.6 m/z window, and fragmentation was achieved via higher-energy collision-induced dissociation (HCD) at 30% normalized collision energy. The MS^2 scan was conducted using an Orbitrap detector at a resolution of 15,000, targeting charge states 2–7 while excluding undetermined charge states. The settings included a maximum injection time of 22 ms, 1 microscan, and a custom AGC target (100% normalized, absolute value 50000). Ions were selected for data-dependent acquisition using an intensity threshold filter of 50000.

Proteomics bioinformatics

MS raw files were processed through Proteome Discoverer v3.0 using the UniProt Mouse Proteome database. A Venn diagram of proteomic data was drawn using Bioladder online tools s (https://www.bioladder.cn/web/). We also performed differential expression protein analysis among protein groups and drew differential volcano maps. The Benjamin Hochberg (BH) method was used to adjust the *p*-value, and enrichment was considered significant when FDR ≤ 0.05. To evaluate the function and signaling pathways of proteins, the online database KOBAS was used to conduct GO and KEGG enrichment analysis. We also selected significant signaling pathways from KEGG (https://www.kegg.jp/kegg/kegg1.html) and acquired a diagram of the signal pathway from the database.

Statistical analysis

All data were expressed as mean ± standard error of the mean (Mean ± SEM). Immunohistochemistry and immunofluorescence results were analyzed using ImageJ, and the Analyze Skeleton (2D/3D) plugin was used for morphological analysis of microglia. Statistical analysis was performed using GraphPad Prism (version 10.0). For multi-group experimental data, one-way analysis of variance (one-way ANOVA) was applied, followed by Tukey's post hoc test for multiple comparisons. For multi-group experimental data with two variables, two-way analysis of variance (two-way ANOVA) was used. All p-value < 0.05 was considered statistically significant.

Data availability

All data generated or analysed during this study are included in this published article (and its supplementary information files), further inquiries can be directed to the corresponding author upon reasonable request.

Received: 25 May 2025; Accepted: 25 August 2025;
Published online: 03 October 2025

References

1. Yamakado, H. et al. Experimental animal models of prodromal Parkinson's disease. *J. Parkinsons Dis.* **14**, S369–S379 (2024).
2. Yuan, Y. et al. Dopaminergic neurodegeneration in the substantia nigra is associated with olfactory dysfunction in mice models of Parkinson's disease. *Cell Death Discov.* **9**, 388 (2023).
3. Bang, Y. et al. Recent advances in the pathology of prodromal non-motor symptoms olfactory deficit and depression in Parkinson's disease: clues to early diagnosis and effective treatment. *Arch. Pharmacal Res.* **44**, 588–604 (2021).
4. Spillantini, M. G. et al. α-synuclein in filamentous inclusions of Lewy bodies from Parkinson's disease and dementia with Lewy bodies. *Proc. Natl Acad. Sci. USA* **95**, 6469–6473 (1998).
5. Taguchi, T. et al. α-Synuclein BAC transgenic mice exhibit RBD-like behaviour and hyposmia: a prodromal Parkinson's disease model. *Brain* **143**, 249–265 (2020).
6. Spillantini, M. G. et al. Alpha-synuclein in Lewy bodies. *Nature* **388**, 839–840 (1997).
7. Braak, H. et al. Staging of brain pathology related to sporadic Parkinson's disease. *Neurobiol. Aging* **24**, 197–211 (2003).
8. Hawkes, C. H. et al. Parkinson's disease: a dual-hit hypothesis. *Neuropathol. Appl Neurobiol.* **33**, 599–614 (2007).
9. Rey, N. L. et al. Spread of aggregates after olfactory bulb injection of α-synuclein fibrils is associated with early neuronal loss and is reduced long term. *Acta Neuropathologica* **135**, 65–83 (2017).
10. Langston, J. W. et al. Chronic Parkinsonism in humans due to a product of meperidine-analog synthesis. *Science* **219**, 979–980 (1983).
11. Prediger, R. D. S. et al. Single intranasal administration of 1-methyl-4-phenyl-1,2,3,6-tetrahydropyridine in C57BL/6 mice models early preclinical phase of Parkinson's disease. *Neurotox. Res.* **17**, 114–129 (2009).
12. Prediger, R. D. S. et al. The risk is in the air: Intranasal administration of MPTP to rats reproducing clinical features of Parkinson's disease. *Exp. Neurol.* **202**, 391–403 (2006).
13. Rojo, A. I. et al. Persistent penetration of MPTP through the nasal route induces Parkinson's disease in mice. *Eur. J. Neurosci.* **24**, 1874–1884 (2006).
14. Srinivasan, K. Biological activities of red pepper (capsicum annuum) and its pungent principle capsaicin: A review. *Crit. Rev. Food Sci. Nutr.* **56**, 1488–1500 (2016).
15. Mózsik, G. et al. Interdisciplinary review for correlation between the plant origin capsaicinoids, non-steroidal antiinflammatory drugs, gastrointestinal mucosal damage and prevention in animals and human beings. *Inflammopharmacology* **17**, 113–150 (2009).
16. Petran, E. M. et al. Capsaicin: emerging pharmacological and therapeutic insights. *Curr. Issues Mol. Biol.* **46**, 7895–7943 (2024).
17. Boiangiu, R. S. et al. Insights into pharmacological activities of nicotine and 6-Hydroxy-L-nicotine, a bacterial nicotine derivative: A systematic review. *Biomolecules*. **14**, (2024).
18. Stolberg, V. B. A cross-cultural and historical survey of tobacco use among various ethnic groups. *J. Ethn. Subst. Abus.* **6**, 9–80 (2008).
19. Quik, M. et al. Nicotine reduces established levodopa-induced dyskinesias in a monkey model of Parkinson's disease. *Mov. Disord.* **28**, 1398–1406 (2013).
20. Dasgupta, P. et al. Nicotine inhibits apoptosis induced by chemotherapeutic drugs by up-regulating XIAP and survivin. *Proc. Natl Acad. Sci.* **103**, 6332–6337 (2006).
21. Lee, J.-G. et al. Combined treatment with capsaicin and resveratrol enhances neuroprotection against glutamate-induced toxicity in mouse cerebral cortical neurons. *Food Chem. Toxicol.* **50**, 3877–3885 (2012).

22. Bok, E. et al. Modulation of M1/M2 polarization by capsaicin contributes to the survival of dopaminergic neurons in the lipopolysaccharide-lesioned substantia nigra in vivo. *Exp. Mol. Med* **50**, 1–14 (2018).
23. Nielsen, S. S. et al. Nicotine from edible solanaceae and risk of Parkinson disease. *Ann. Neurol.* **74**, 472–477 (2013).
24. Akaike, A. et al. Mechanisms of neuroprotective effects of nicotine and acetylcholinesterase inhibitors: Role of α4 and α7 receptors in neuroprotection. *J. Mol. Neurosci.* **40**, 211–216 (2009).
25. Quik, M. et al. Chronic oral nicotine normalizes dopaminergic function and synaptic plasticity in 1-methyl-4-phenyl-1,2,3,6-tetrahydropyridine-lesioned primates. *J. Neurosci.* **26**, 4681–4689 (2006).
26. Kardani, J. et al. Nicotine slows down oligomerisation of α-synuclein and ameliorates cytotoxicity in a yeast model of Parkinson's disease. *Biochimica et. Biophysica Acta (BBA) - Mol. Basis Dis.* **1863**, 1454–1463 (2017).
27. Arthur, J. S. et al. Mitogen-activated protein kinases in innate immunity. *Nat. Rev. Immunol.* **13**, 679–692 (2013).
28. Kim, E. K. et al. Pathological roles of MAPK signaling pathways in human diseases. *Biochimica et. Biophysica Acta (BBA) - Mol. Basis Dis.* **1802**, 396–405 (2010).
29. Yasuda, S. et al. p38 MAP kinase inhibitors as potential therapeutic drugs for neural diseases. *Cent. Nerv. Syst. Agents Med Chem.* **11**, 45–59 (2011).
30. Ratih, K. et al. L-Theanine alleviates MPTP-induced Parkinson's disease by targeting Wnt/β-catenin signaling mediated by the MAPK signaling pathway. *Int J. Biol. Macromol.* **226**, 90–101 (2023).
31. Mutoh, T. et al. Activation of α7 nicotinic acetylcholine receptor augments nerve growth factor action on PCtrk cells. *Toxicology* **509**, 153986 (2024).
32. Chen, Q. et al. Regulation and function of the cGAS-STING pathway of cytosolic DNA sensing. *Nat. Immunol.* **17**, 1142–1149 (2016).
33. Sun, L. J. et al. Cyclic GMP-AMP synthase is a cytosolic DNA sensor that activates the type I interferon pathway. *Science* **339**, 786–791 (2013).
34. Decout, A. et al. The cGAS-STING pathway as a therapeutic target in inflammatory diseases. *Nat. Rev. Immunol.* **21**, 548–569 (2021).
35. Chen, C. et al. Cellular functions of cGAS-STING signaling. *Trends Cell Biol.* **33**, 630–648 (2023).
36. Dhapola, R. et al. cGAS-STING and neurodegenerative diseases: A molecular crosstalk and therapeutic perspective. *Int Immunopharmacol*. **159**, (2025).
37. Ma, C. et al. Microglial cGAS drives neuroinflammation in the MPTP mouse models of Parkinson's disease. *CNS Neurosci. Therapeutics* **29**, 2018–2035 (2023).
38. Liu, Y. Q. et al. 3-N-butylphthalide attenuates neuroinflammation in rotenone-induced Parkinson's disease models via the cGAS-STING pathway. *Int J. Immunopathol. Pharm.* **38**, 1–16 (2024).
39. Marques, N. F. et al. Atorvastatin prevents early oxidative events and modulates inflammatory mediators in the striatum following intranasal 1-methyl-4-phenyl-1,2,3,6-tetrahydropyridine (MPTP) administration in rats. *Neurotox. Res.* **33**, 549–559 (2017).
40. Rui, D. S. Predigera, b. The intranasal administration of 1-Methyl-4-Phenyl-1,2,3,6-Tetrahydropyridine(MPTP): A new rodent odel to test palliative and neuroprotective agents for Parkinson's disease. *Curr. Pharm. Des.* **17**, 489–507 (2011).
41. Tong, Z. Y. et al. Up-regulation of tyrosine hydroxylase mRNA in a sub-population of A10 dopamine neurons in Parkinson's disease. *Mol. Brain Res.* **79**, 45–54 (2000).
42. Subramaniam, S. R. et al. Targeting microglial activation states as a therapeutic avenue in Parkinson's disease. *Front. Aging Neurosci.* **9**, 176 (2017).
43. Moehle, M. S. et al. M1 and M2 immuneactivation in Parkinson's Disease:foe and ally?. *Neuroscience* **302**, 59–73 (2015).
44. Han, X. J. et al. Nicotine alleviates cortical neuronal injury by suppressing neuroinflammation and upregulating neuronal PI3K-AKT signaling in an eclampsia-like seizure model. *Neurotox. Res.* **38**, 665–681 (2020).
45. Han, T. H. et al. Capsaicin inhibits HIF-1α accumulation through suppression of mitochondrial respiration in lung cancer cells. *Biomed. Pharmacother.* **146**, 112500 (2022).
46. Ransohoff, R. M. A polarizing question: Do M1 and M2 microglia exist?. *Nat. Neurosci.* **19**, 987–991 (2016).
47. Wolf, S. A. et al. Microglia in physiology and disease. *Annu Rev. Physiol.* **79**, 619–643 (2017).
48. Kim, E. K. et al. Compromised MAPK signaling in human diseases: an update. *Arch. Toxicol.* **89**, 867–882 (2015).
49. Huang, Y. G. et al. Mechanism and therapeutic potential of targeting cGAS-STING signaling in neurological disorders. *Mol. Neurodegener.* **18**, 79 (2023).
50. Sliter, D. A. et al. Parkin and PINK1 mitigate STING-induced inflammation. *Nature* **561**, 258–262 (2018).
51. Prediger, R. D. S. et al. Risk is in the air: An intranasal MPTP (1-Methyl-4-Phenyl-1,2,3,6-Tetrahydropyridine) rat model of Parkinson's Disease. *Ann. N. Y Acad. Sci.* **1170**, 629–636 (2009).
52. Biju, K. C. et al. Methylene blue ameliorates olfactory dysfunction and motor deficits in a chronic MPTP/probenecid mouse model of Parkinson's Disease. *Neuroscience* **380**, 111–122 (2018).
53. Yang, J. et al. Nicotine improved the olfactory impairment in MPTP-induced mouse model of Parkinson's disease. *Neurotoxicology* **73**, 175–182 (2019).
54. Chen, F. et al. -Synuclein aggregation in the olfactory bulb induces olfactory deficits by perturbing granule cells and granular–mitral synaptic transmission. *npj Parkinson's Dis.* **7**, 114 (2021).
55. Chung, Y. C. et al. Capsaicin prevents degeneration of dopamine neurons by inhibiting glial activation and oxidative stress in the MPTP model of Parkinson's disease. *Exp. Mol. Med* **49**, 1–9 (2017).
56. Thacker, E. L. et al. Temporal relationship between cigarette smoking and risk of Parkinson's disease. *Neurology* **68**, 764–768 (2007).
57. Siddique, Y. H. et al. Effect of capsaicin on the oxidative stress and dopamine content in the transgenic Drosophila model of Parkinson's disease. *Acta Biol. Hung.* **69**, 115–124 (2018).
58. Quik, M. et al. Potential therapeutic application for nicotinic receptor drugs in movement disorders. *Nicotine Tob. Res.* **21**, 357–369 (2019).
59. Okada, K. et al. Nicotine exerts a stronger immunosuppressive effect than its structural analogs and regulates experimental colitis in rats. *Biomedicines* **11**, 922 (2023).
60. Doty, R. L. Olfactory dysfunction in Parkinson disease. *Nat. Rev. Neurol.* **8**, 329–339 (2012).
61. Poewe, W. et al. Parkinson disease. *Nat. Rev. Dis. Prim.* **3**, 17013 (2017).
62. Klein, M. O. et al. Dopamine: functions, signaling, and association with neurological diseases. *Cell Mol. Neurobiol.* **39**, 31–59 (2019).
63. Bohnen, N. I. et al. Selective hyposmia and nigrostriatal dopaminergic denervation in Parkinson's disease. *J. Neurol.* **254**, 84–90 (2007).
64. Liu, S. L. Dopaminergic modulation of glomerular circuits in the mouse olfactory bulb. *Front. Cell. Neurosci.* **14**, 172 (2020).
65. Fullard, M. E. et al. Olfactory dysfunction as an early biomarker in Parkinson's Disease. *Neurosci. Bull.* **33**, 515–525 (2017).
66. Doty, R. L. et al. Bilateral olfactory dysfunction in early stage treated and untreated idiopathic parkinson's disease. *J. Neurol. Neurosurg. Psychiatry* **55**, 138–142 (1992).
67. Carnevale, D. et al. Microglia-neuron interaction in inflammatory and degenerative diseases: role of cholinergic and noradrenergic systems. *CNS Neurol. Disord. Drug Targets* **6**, 388–397 (2007).
68. Saporito, M. S. et al. MPTP activates c-Jun NH_2-terminal kinase terminal kinase (JNK) and its upstream regulatory kinase MKK4 in nigrostriatal neurons in vivo. *J. Neurochemistry* **75**, 1200–1208 (2000).
69. Xia, X. G. et al. Gene transfer of the JNK interacting protein-1 protects dopaminergic neurons in the MPTP model of Parkinson's disease. *Proc. Natl Acad. Sci. USA* **98**, 10433–10438 (2001).

70. Rai, S. N. et al. The role of PI3K/Akt and ERK in neurodegenerative disorders. *Neurotox. Res.* **35**, 775–795 (2019).
71. Silva, R. M. et al. Mixed lineage kinase–c-jun N-terminal kinase signaling pathway: A new therapeutic target in Parkinson's disease. *Mov. Disord.* **20**, 653–664 (2005).
72. Mathiasen, J. R. et al. Inhibition of mixed lineage kinase 3 attenuates MPP^+-induced neurotoxicity in SH-SY5Y cells. *Brain Res.* **1003**, 86–97 (2004).
73. Yu, T. et al. The pivotal role of TBK1 in inflammatory responses mediated by macrophages. *Mediators Inflamm.* **2012**, 979105 (2012).
74. Zhang, Y. et al. The cGAS-STING pathway drives neuroinflammation and neurodegeneration via cellular and molecular mechanisms in neurodegenerative diseases. *Neurobiol. Dis.* **202**, 106710 (2024).
75. Paul, B. D. et al. Signaling by cGAS-STING in neurodegeneration, neuroinflammation, and aging. *Trends Neurosci.* **44**, 83–96 (2021).
76. Cain, W. S. Odor identification by males and females: predictions vs performance 1. *Chem. Senses* **7**, 129–142 (1982).
77. Hummel, T. et al. Normative data for the "Sniffin' Sticks" including tests of odor identification, odor discrimination, and olfactory thresholds: an upgrade based on a group of more than 3000 subjects. *Eur. Arch. Oto-Rhino-Laryngol.* **264**, 237–243 (2006).
78. Doty, R. L. et al. Development of the university of pennsylvania smell identification test: A standardized microencapsulated test of olfactory function. *Physiol. Behav.* **32**, 489–502 (1984).
79. Fleming, S. M. et al. Olfactory assays for mouse models of neurodegenerative disease. *J. Vis. Exp.* **90**, e51804 (2014).
80. Liu, D. et al. Medial prefrontal activity during delay period contributes to learning of a working memory task. *Science* **346**, 458–463 (2014).
81. Feng, Y. et al. Photobiomodulation inhibits ischemia-induced brain endothelial senescence via endothelial nitric oxide synthase. *Antioxidants* **13**, 633 (2024).
82. Feng, Y. et al. Activation of testosterone-androgen receptor mediates cerebrovascular protection by photobiomodulation treatment in photothrombosis-induced stroke rats. *CNS Neurosci. Therapeutics* **30**, e14574 (2024).

Acknowledgements

This research was funded by the National Natural Science Foundation of China (Grant No. 82101506, 32272455, 32072344), the China Postdoctoral Science Foundation (Grant No. 2023M733887), and the scientific project of Beijing Life Science Academy (Grant No. 2023000CC0140, 2023000CB0010, 2024301QPIA01). We thank Dr. Chuanhui Han for the professional guidance of the research. We thank Dr. Yunhe Zhu, Mengjiao Li, Xiaomei Jiao and Can Qiao for technical support in the research.

Author contributions

J.W. performed most of the experiments, prepared the figures, interpreted the data, and wrote the manuscript. J.X. conducted the supervision and project administration. Y.X. and J.M. conceived and designed the experiments and contributed to the writing, editing, review and project administration. L.W. and L.G. performed quantitative proteomics. W.C., M.R., S.R., S.N. and Z.X. performed the animal experiments. H.H., Y.Z. and F.G. performed the interpretation of data. D.W., Y.L. and H.Y. contributed to the methodology and formal analysis. All authors reviewed the manuscript.

Competing interests

The authors declare no competing interests.

Additional information

Supplementary information The online version contains supplementary material available at https://doi.org/10.1038/s41531-025-01135-4.

Correspondence and requests for materials should be addressed to Jian Mao or Yan Xu.